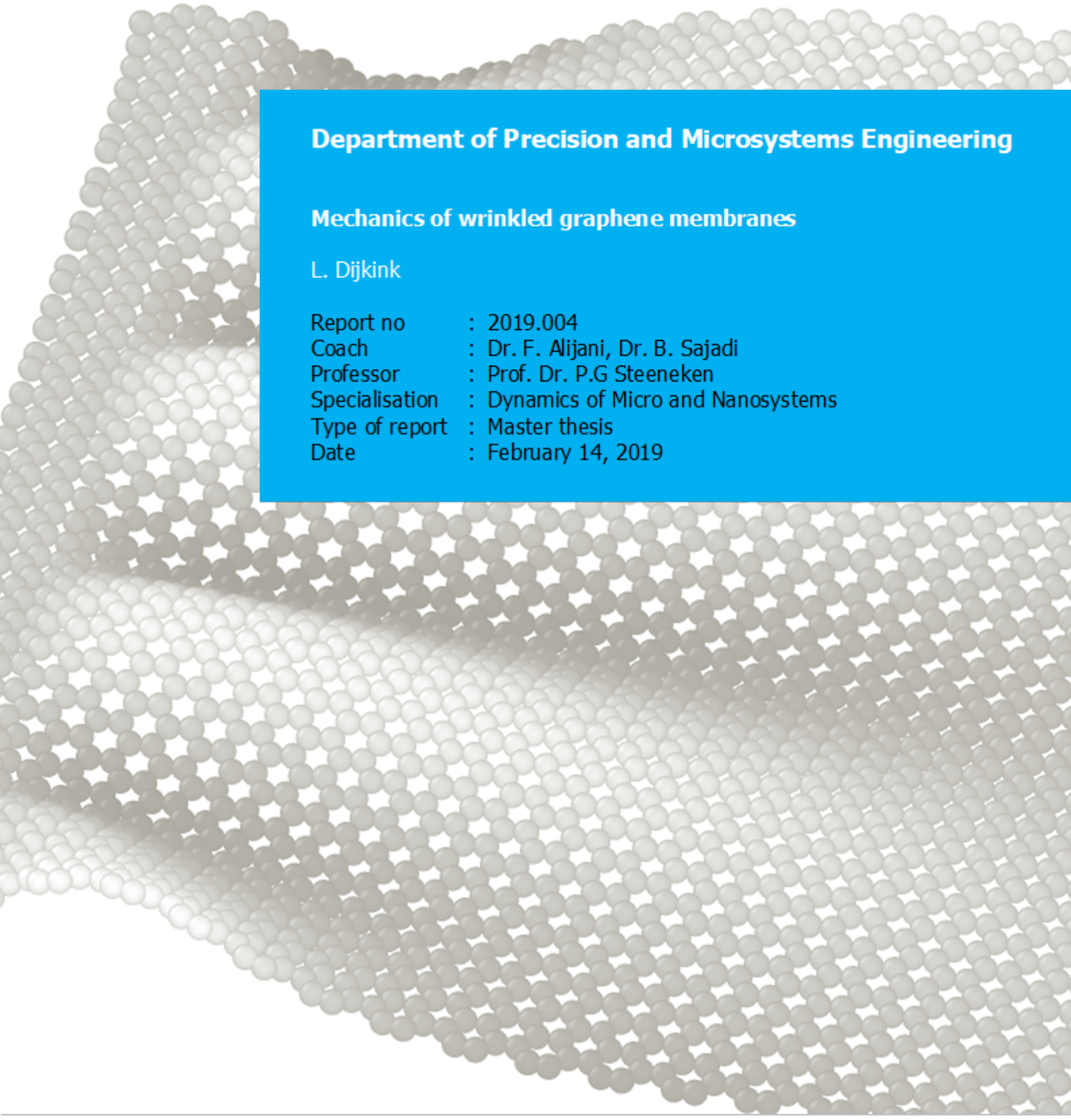

Department of Precision and Microsystems Engineering

Mechanics of wrinkled graphene membranes

L. Dijkink

Report no : 2019.004
Coach : Dr. F. Alijani, Dr. B. Sajadi
Professor : Prof. Dr. P.G Steeneken
Specialisation : Dynamics of Micro and Nanosystems
Type of report : Master thesis
Date : February 14, 2019

Mechanics of wrinkled graphene membranes

by

L. Dijkink

to obtain the degree of Master of Science
at the Delft University of Technology,
to be defended publicly on February 14, 2019 at 10:00 AM.

Student number:	4222865	
Project duration:	January 18, 2018 - February 14, 2019	
Thesis committee:	Prof. dr. P. G. Steeneken,	TU Delft, DMN, chair
	Dr. F. Alijani,	TU Delft, DMN, supervisor
	Dr. C. Ayas,	TU Delft, SOM, external examiner

An electronic version of this thesis is available at `http://repository.tudelft.nl/`.

TU Delft

Preface

Before you lies my master thesis report, which is the final part of my Master of Science in Mechanical Engineering at Delft University of Technology. This work has been executed at the Dynamics of Micro and Nanosystems (DMN) group at the department of Precision and Microsystems Engineering (PME) at the Mechanical, Maritime and Materials Engineering (3mE) faculty. It describes the research I carried out in this group, aimed to gain a better understanding of the mechanics of wrinkled graphene membranes.

I would like to express my gratitude to my supervisors, Banafsheh Sajadi and Farbod Alijani, for their sincere support, extensive knowledge and guidance during the project. Closely related I would like to thank the entire DMN group, staff and the other master students for providing the stimulating and relaxed atmosphere.

Lastly,I would like to express my gratitude to my friends and family for supporting me each in their own way during this project and really throughout my whole studies and life.

L. Dijkink
Delft, February 2019

Summary

The outstanding mechanical properties of graphene have made it a suitable candidate for a wide range of sensor and actuator applications in modern technology. However, before the full potential of future applications can be achieved, a proper characterisation of the fundamental properties of graphene is crucial. The aim of this project was to contribute to the understanding of the mechanics of graphene membranes in presence of surface imperfections. To this end two configurations are investigated: ribbons and cantilevers, respectively.

Wrinkled graphene nanoribbons are used to investigate the mechanical behaviour during the transition from the wrinkled state to the flat state. A molecular dynamics model has been developed of a single layer graphene ribbon to describe both the formation of wrinkles as well as the transition from the wrinkled state to the flat state. Also, a continuum model was developed to investigate the formation of wrinkles in graphene nanoribbons. Different constitutive laws have been investigated to describe the mechanical response of wrinkled membranes during the transition from the wrinkled state to the flat state. It was concluded that an exponential version of Hooke's law fails to describe this transition correctly. The transition is however well described by the first order compressible Ogden's law. Ogden's law provided further insights into different mechanical properties of the wrinkled layer. Ogden's law predicted that wrinkled membranes exhibit a negative Poisson's ratio at small strains, which is in agreement with previous research. Also, Ogden's law predicted a decreasing shear modulus and an increasing Poisson's ratio after flattening of the membrane.

Single layer graphene cantilevers show great potential, however, due to the difficult manufacturing of these fragile structures they remain virtually unstudied. Herein, a molecular dynamics model has been developed to investigate if nanocantilevers could be stabilised by implying a curvature. We found that, depending on the aspect ratio of the membrane and the applied rate of curvature, single layer graphene cantilevers could be (partly) stabilised by implying a curvature.

In conclusion, with this research we provided new insights for designing and investigating the next generation of graphene nanoelectromechanical devices.

Contents

I

Introduction

1 Introduction

The Nobel Prize in Physics 2010 was awarded to Andre Geim and Konstantin Novoselov. In 2004 they were the first able to isolate graphene with a thickness of only one atom [1]. Since 2004 graphene exploration has accelerated fast, in almost every field of science and engineering research have been performed on graphene. This enormous interest in graphene is mainly due to the unique structure of graphene and the exceptional physical and chemical properties. Research showed that graphene is the strongest material known and it has outstanding conductive properties for example. These exceptional properties make graphene interesting for both fundamental studies and future applications. However, before the full potential of future applications can be achieved, a proper characterisation of the fundamental properties of graphene membranes is crucial. Over the years a lot of properties have been investigated on graphene samples with a high degree of perfection of the atomic lattice. Nonetheless, mono-layer graphene shows a lot of imperfections. During growth or processing structural defects can appear. Next to structural defects, surface corrugations like wrinkling and rippling occur in single layer graphene sheets. Recent experiments have suggested significant effects of both types of imperfections on the mechanical properties of graphene [3]. Knowing the mechanical properties of graphene and the effects of changes in the structure are of extreme importance to investigate the possible applications of graphene.

Although a lot of research has been done, surface imperfections in graphene are still relatively unexplored. This research aims to develop a better understanding of the mechanics of graphene membranes in presence of surface imperfections.

This research is performed in the following structure: In the first part an introduction to the subject of this research is given. In chapter 2 an introduction to graphene is presented. Additionally, the current state of research, regarding imperfections in graphene, is discussed. Furthermore, relevant modelling techniques are presented. In chapter 3 the research question, research objectives and research methodology are presented. In the next part, part II, the findings on the effects of surface imperfections on rectangular ribbons and cantilevers are presented. Finally, in part III, conclusions are drawn based on the obtained knowledge and ideas for further research are discussed in chapter 6.

2

Literature review

This chapter is intended to introduce the reader to the research topic, to present the current state of research and research gaps identified. First an introduction into the properties of graphene is given. Additionally, the current state of research, regarding imperfections in graphene, is discussed. Furthermore, relevant modelling techniques are presented. This review is a summary of the broader literature review performed by the author, readers interested in a more extensive overview could read the full version of the literature review.

2.1. Introduction to graphene

Graphene is an one-atom thick, two-dimensional sheet of carbon atoms. In structurally perfect graphene sheets, named pristine, atoms are densely packed in a hexagonal crystal lattice bonded by covalent bonds, as can be seen in figure 2.1. These covalent bonds are strong triangular σ-type bonds of the sp^2-hybridised orbitals, hence every atom is bonded with four bonds: one σ-bond with each of its neighbours and one π-bond that is oriented out-of-plane. The free π-bonds are responsible for thermal fluctuations which stabilise freestanding graphene, resulting in ripples, first observed by Meyer *et al.* [45, 50].

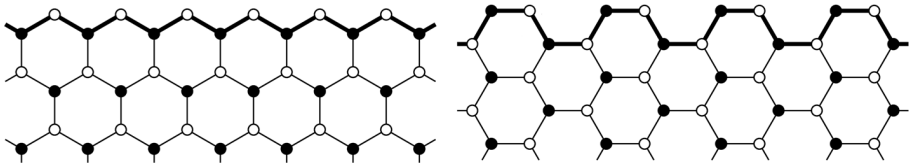

Figure 2.1: Hexagonal lattices of graphene, with two types of edges, indicated by bold line: zigzag edge (left) and armchair edge (right). Image from [58].

Producing pristine graphene on a large scale is a major challenge. High quality methods, such as mechanical exfoliation and synthesis on SiC, can only be used in fundamental research and niche applications because of the limited scalability. Scalable methods, like liquid-phase exfoliating, are very expensive and the yield of the overall production process is low [60]. It can be stated that during the production process structural defects inevitable occur in graphene.

2.1.1. Properties of graphene

A number of researchers have reported on the exceptional properties of graphene. The properties are related to the different structural characterisations of graphene. It must be pointed out that all the properties have been extracted from research performed on pristine graphene.

Electronics Both experiments and theory showed that graphene has a very high electron mobility. Mayorov *et al.* [44] experimentally measured values up to $2.5 \times 10^5\,\mathrm{cm^2\,V^{-1}\,s^{-1}}$ at room temperature. Furthermore, Novoselov *et al.* [54] stated that this mobility is independent of temperature between 10 K and 100 K . The high electron mobility of graphene can be explained by the type of hybridisation of the bonds. The sp^2-hybridisation leaves one electron freely available in the third dimension for electronic conduction.

Thermal The in-plane thermal capacity of graphene at room temperature is among the highest of any known material. Balandin *et al.* [23] obtained values up to $\sim 5300\,\mathrm{W\,m^{-1}\,K^{-1}}$. However these extremely high values have been questioned by Chen *et al.* [15]. Nevertheless, the high thermal capacity of graphene can be explained by the type of hybridisation, sp^2. The free bonds create lattice vibrations, which result in efficient heat transfer [7].

Another special thermal property of graphene is the negative thermal expansion coefficient (TEC) at low temperatures [48], caused by dynamic rippling. Gao and Huang [21] showed that at higher temperatures the rippling is suppressed by anharmonic interactions and therefore a positive thermal expansion occurs. Researchers nowadays agree on the existence of a negative TEC, however the reported transition temperatures are inconsistent.

Optical Research performed by Brownson *et al.* [13] revealed that graphene has a very high optical transparency, up to 97.7 %. This optical transparency is decreasing linearly with the addition of more layers [65]. The high transparency can be explained by the fact that graphene is consisting of only one layer of atoms.

Mechanical Experimental measurements and numerical studies of the mechanical properties of pristine graphene reported values of around 1 TPa for the Young's modulus, the fracture strength to be 130 GPa and a breaking strength of $42\,\mathrm{N\,m^{-1}}$ [30, 32, 37]. The studies of both [30] and [37] assumed a linear stress-strain behaviour at small strains. However, the experimental research performed by [32] suggested nonlinear stress-strain behaviour as well. Different researchers suggested that this nonlinear stress-strain behaviour at small strains is caused by surface corrugations like thermal rippling, static wrinkling and crumpling [21, 34, 52]. The high in-plane stiffness can be explained by the perfect hexagonal lattice and the carbon-carbon bonds [3].

Although it is assumed that graphene has a low bending rigidity, there is still a large spread in the theoretical predictions of this bending rigidity [35, 76]. Classic plate theory cannot be applied to define the bending rigidity of graphene, since the bending moduli of monolayer graphene are not directly related to the in-plane Young's modulus and Poisson's ratio. The bending moduli of single layer graphene are resulting from interactions among the carbon atoms [39]. The low bending rigidity can be explained by the fact that graphene is only one layer thick, and therefore very thin.

A review performed by Akiwande *et al.* [3] showed that there is still a large spread in theoretical predictions of the Poisson's ratio of graphene. Jian *et al.* [28] investigated the intrinsic negative Poisson's ratio (NPR) of single-layer graphene sheets. They showed that this NPR is independent of the size and temperature of the layer . On the other side research showed that as a result of thermal rippling, the positive Poisson's ratio can change to a negative Poisson's ratio at higher temperatures [24, 81].

Based on the above review it can be stated that graphene has exceptional properties in different areas. Nonetheless, spread in theoretical predictions of the different properties still exists. Furthermore, it has been shown that all these properties are dependent on the structure of graphene, it was already suggested that structural as well as surface imperfections could possibly influence the properties.

2.2. Imperfections in single layer graphene

It was outlined that imperfections are inevitable in graphene layers. In the last years a tremendous progress has been achieved in understanding the formation mechanisms of defects and their effects on the mechanical properties of graphene.

2.2.1. Structural defects

Structural defects are defined as changes in the atomic structure. Structural defects will inevitably occur in graphene, because of imperfections in the production process or because of operation conditions of the graphene device.

Structural defects are categorised based on their dimensionality. Lattice defects that occur around or at a single lattice point are point-defects. Different types of point-defects can be seen in figure 2.2. Dislocations are combinations of point-defects, like vacancies or adatoms. Grain boundaries are extensions of dislocations, since multiple dislocations can result in a grain boundary. It should be pointed out that in the end an infinite number of lattice defects can occur, however, this review will only consider the simplest ones.

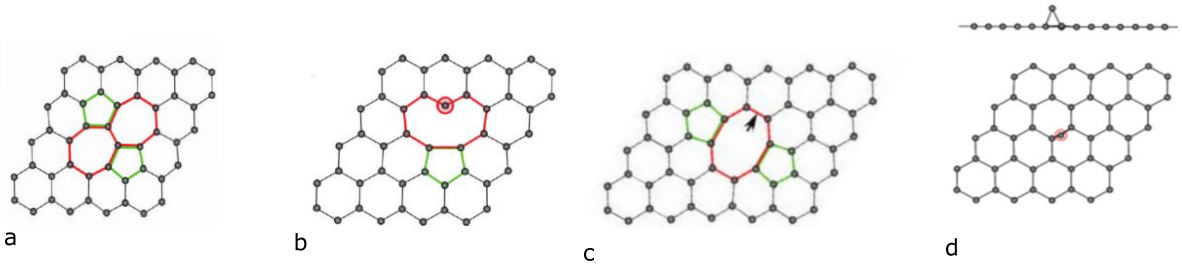

Figure 2.2: Point-defects in single layer graphene obtained from DFT calculations: a) STW-defect, b) single vacancy, c) (5-8-5) type double vacancy, d) carbon adatom in bridge configurations. Images from [8].

Stone-Thrower-Wales defect A widely investigated point defect is the Stone-Wales defect (SW-defect), also named the Stone-Thrower-Wales defect [66]. In this type of defect the carbon-carbon bond is rotated in-plane with 90°, the lattice is therefore rearranged by forming non-hexagonal rings, as can be seen in figure 2.2a. Research showed that the SW-defect slightly effects the Young's modulus. The failure strain and intrinsic strength are significantly reduced [5, 20, 74]. An increasing density of SW-defects result in a bigger change in the aforementioned mechanical properties [47].

Theoretically it was predicted that the heptagons and pentagons formed could induce curvature [69]. Curvature around SW-defects has been shown by Ma *et al.* [41] using density functional theory and quantum Monte Carlo simulations.

Vacancy type defects In vacancy type defects atoms are removed from the lattice, as can be seen in figure 2.2b. Since single vacancies are not rigid, they can recombine with another vacancy and stabilise by forming a multiple vacancy, were multiple atoms are missing [33].

A higher density of vacancies will result in a bigger reduction of the effective elastic modulus, independent of the location of the vacancy. Also, the effects of vacancy type defects on the elastic modulus are greater than the effects of SW-defects [47, 68]. Ab initio calculations performed by Fedorov *et al.* [19] resulted in the same correlation between the density of vacancies and the reduction of the elastic modulus. Moreover, Tapia *et al.* [68] showed that single-vacancies result in a decrease of the shear modulus. Wang *et al.* [74] showed that vacancies reduce the fracture strength of graphene layers. Also, since heptagons and pentagons could be formed, surface corrugations could occur.

Adatoms In adatom type of defects the lattice absorbed another atom, which is called an adatom. This absorption can appear in different configurations, so called hollow, bridge and top configurations, as can be seen in figure 2.3. The bridge and top configurations result in a coarse surface. Besides the different configurations, different types of atoms can be absorbed. The effect on the mechanical properties of graphene of this defect is depending on the type of adatom. For example, carbon adatoms change the hybridisation of the carbon atoms in the layer. Sp^2-hybridisation can change to sp^3-hybridisation [8]. Since the sp^3-hybridisation is weaker than sp^2-hybridisation, this layer will be weaker.

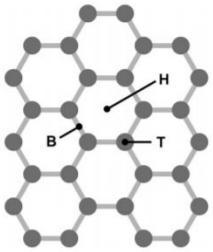

Figure 2.3: Different adsorption configurations: hollow (H), bridge (B) and top (T). Image from [42].

Substitutional impurity In substitutional impurity type of defects foreign atoms are incorporated into the graphene layer. Since the bond-lengths between carbon and other atoms differ from the carbon-carbon bond, surface corrugations will occur. As has been stated for adatom-type of defects, the effects of impurities on the mechanical properties are depending on the type of foreign atoms.

Line defects Lattice defects which occur around or at multiple lattice points are line defects, different types of line defects can be seen in figure 2.4. Dislocations are combinations of point defects, like vacancies or adatoms. Grain boundaries are extensions of dislocations, since multiple dislocations can result in a grain boundary.

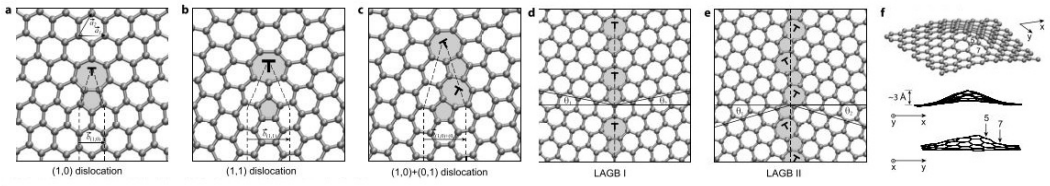

Figure 2.4: Atomic structures of different types of line defects. From left to right: (1,0) dislocation, (1,1) dislocation, (1,0)+(0,1) dislocation pair, large-angle grain boundary of the $\theta = 21.8°$ type, large-angle grain boundary of $\theta = 21.8°$ type, buckling of the graphene layer caused by the (1,0) dislocation. Image from [80].

Research showed that dislocations result in surface corrugations, named wrinkles. These wrinkles can be seen in the most right figure of figure 2.4. It has already been shown that a higher density of point defects results in a bigger reduction of the Young's modulus. In line with this statement, it could be stated that the effects of line defects on the mechanical properties are depending on the type of point defects of which they are build of. Experimental research performed by Ruiz-Vargas [63] showed that cracks propagate along the zigzag and armchair directions, not along the grain boundaries . Zhang *et al.* [83] investigated the effect of buckling induced by the grain boundaries. They showed that the grain boundaries with high thermodynamic stability can be almost as strong as pristine graphene.

In summary it can be seen that the properties of graphene are affected by structural defects. Next to changes in mechanical properties, it was stated that structural defects can result in surface corrugations. The next section will focus on the effects of surface corrugations on the mechanical properties of graphene.

2.2.2. Surface imperfections

Surface imperfections are defined as changes in the flatness of the surface. Different types of surface imperfections could occur in graphene. Figure 2.5 shows the three different types: dynamic rippling, static wrinkling and crumpling.

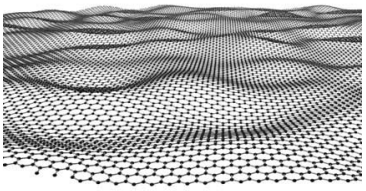

(a) Rippled graphene, image from [45].

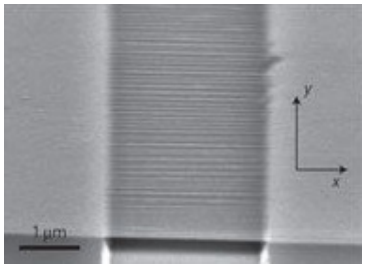

(b) Wrinkled graphene, image from [9].

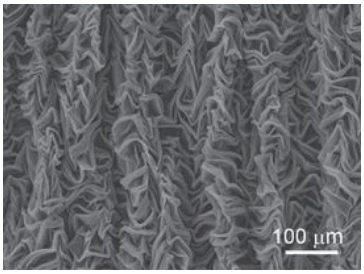

(c) Crumpled graphene, image from [82].

Figure 2.5: Surface imperfections in single layer graphene.

Rippling Strictly 2D crystals are thermodynamically unstable, and therefore corrugations should exist to stabilise the layer. Xu *et al.* [79] showed via scanning tunnelling microscopy that ripples are not static, but dynamically change with time.

Multiple studies investigated the effects of ripples on the mechanical behaviour of graphene. It has been shown that ripples result in nonlinear stress-strain behaviour at small strains. Also, it was observed that the ripple amplitude decreases rapidly when strain increases [21, 34, 61].

Next to the effects of ripples on the stress-strain behaviour of graphene, studies showed significant effects of temperature on the ripple behaviour and therefore on the mechanical behaviour. Results showed that the maximum as well as the initial elasticity decreases almost linearly if the temperature increases. This reduction is caused by the increasing out-of-plane displacement [21, 34, 85]. Monte Carlo simulations of Chen and Chrzan [16] also showed that the Young's modulus significantly decreases with increasing temperature, because of the increasing ripple amplitude. Ramirez *et al.* [62] showed an increasing bending rigidity when the temperature is increased. Zakharchenko *et al.* [81] showed that at around 1700 K the positive Poisson's ratio changes to a negative Poisson's ratio, because of the increasing ripple amplitude. Studies also revealed that ripples effect the thermal expansion coefficient of graphene. Since the out-of-plane atomic vibrations are energetically favoured over in-plane vibrations, graphene has a negative thermal expansion at low temperatures, and a positive thermal expansion at higher temperatures [21]. Studies disagree on the transition temperature, so the point where the negative TEC is changed to a positive TEC.

Wrinkling Another type of surface imperfections is wrinkling. Wrinkles can be seen in graphene layers as manifestations of local buckling resulting in different static wrinkle patterns, as can be seen in figure 2.6. Different mechanisms can induce wrinkle formation in graphene layers. In general, wrinkles are formed in graphene layers when the layer is under uneven stresses resulting in a strain higher than the critical strain needed to induce the local buckling [14].

A common cause is the interaction between the substrate and the graphene layer. Obratztsov *et al.* [55] showed that when graphene is cooled after the CVD process the horizontal length of the graphene sheet increases, because of a reduction of flexural modes. When the metal substrate, in this case nickel, is cooled it will shrink. This difference in thermal expansion coefficients between graphene and the underlying substrate results in stresses, which will induce wrinkles. Furthermore, research showed that when substrates are not perfectly flat, larger types of wrinkles will occur in the graphene layer [38]. Wrinkles can also be induced during the exfoliation process. If the pressure is removed and the pinning energy to the substrate is low, wrinkles are formed to reduce the elastic energy in the layer [25]. After the graphene layer is exfoliated on the metal substrate it is transferred to another substrate for further use. Depending on the type of transfer medium wrinkles can be released or preserved [38].

Wrinkles can also occur in freestanding graphene samples by applying tension, compression or shear [14, 17, 49]. Min and Aluru [46] showed that the wrinkling amplitude is depending on the amount of shear strain,

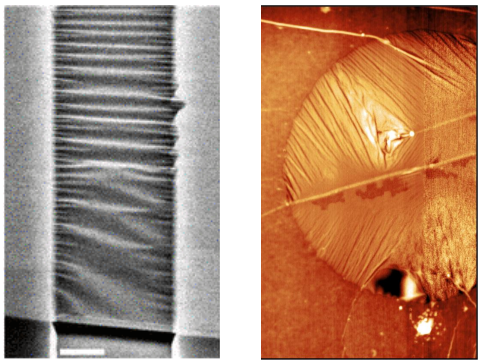

Figure 2.6: Wrinkles seen in experiments of graphene: a) Scanning electron microscopy image of bilayer suspended graphene sheet. Images from [71]. b) Circular membrane with wrinkles, M. Šiškins (2018).

but almost independent of temperature. The amplitude will increase when the shear strain is increasing. The observations of Duan *et al.* [17] build upon this observation. They showed that the amplitude of the wrinkles increases first with increasing strain, after which the amplitude will become stable. A last important origin of wrinkles are structural defects. The formation of heptagons and pentagons can result in surface corrugations.

Research on the effects of wrinkles, caused by atomic mismatches at the boundaries, on the mechanical properties of graphene showed nonlinear behaviour at small strains [83]. Research on the influence of defect induced wrinkles on the Poisson's ratio of graphene showed a negative Poisson's ratio [24, 59]. It should be noted that although these studies focused on the effects of wrinkling, ripples also occurred since most of the research is performed at temperatures above 0 K, and therefore ripples affected the properties of graphene as well.

Crumpling Crumples can be seen in graphene as folds and wrinkles in two and three dimensions. Crumpling is a process which can result in a total new geometry of the graphene layer. Different formation mechanisms will result in different structures, as can be be seen in figure 2.7. Static wrinkling and dynamic flexural phonons are the origin of crumples in freestanding graphene [51].

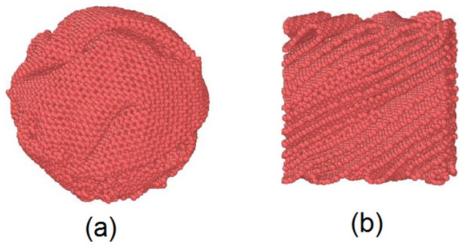

Figure 2.7: Different structures of crumpled graphene. a) Structure after hydrostatic compression. b) Structure after biaxial compression. Image from [72].

Since the final structures generated during the crumpling process are different, the properties of crumpled graphene will differ. This section will review a few of the structures.

Nicholl *et al.* [51] experimentally investigated lightly crumpled sheets of graphene. The research showed that graphene is significantly softened by the combination of wrinkles and ripples. Furthermore, the contribution of wrinkles to the softening behaviour is dominant over flexural phonons. Also, the nonlinear behaviour seen in rippled and wrinkled graphene has been observed. Observations made clear that a higher amount of crumpling will result in a higher degree of nonlinearity.

Luo *et al.* [40] experimentally investigated paperball-like graphene-oxide (GO) structures. Their research showed that crumpled GO-balls show increased stiffness and strength when compressed. An increase in plastic deformation will result in a higher stiffness.

2.3. Modelling dynamic properties of graphene

Over the years a lot of research has been performed on the different properties of graphene. A lot of research is performed by experiments, however, as mentioned by van Hemert [26], there are three main issues in experimental research. First, controlling the environment can be hard. Second, fabricating high quality graphene membranes is still difficult. And third, measuring becomes very hard at the atomic scales, as the eigenfrequencies enter the GHz regime. Consequently, a lot of research on graphene has been performed on an abstract level, using analytic models and atomistic simulations. Understanding of the different modelling approaches is important to make a considered decision on which techniques could be used in further research to imperfections. The different modelling techniques can be categorised into different sections, according to their time and scale constraints. In this brief study on the different methods most of the methods are treated as separate methods, however combinations of the different methods are possible. For example, molecular dynamics with an quantum mechanics potential. Since a lot of different combinations are possible, not all combinations are presented.

Quantum mechanics Quantum mechanics (QM) describes the properties of graphene at the smallest scale directly from theoretical principles. The quantum mechanical wave function, the Schrödinger equation, is used to find the solutions. This quantum mechanical wave-function contains all the information about a given system. By integrating this equation over time the dynamic behaviour is found. For larger many-body system the Schrödinger equation is too complex to be numerically solved, therefore simplifications are applied to the Schrödinger equation. For example the Hartree-Fock method, an ab initio method assuming the wave-function by a single Slater determinant made up on one spin orbital per electron. Another example is the density function theory (DFT), based on the electron density function. Other simplications are semi-empirical methods which obtain multiple parameters from empirical data.

Kudin *et al.* [30] and Liu *et al.* [37] used DFT to obtain the Young's modulus and Poisson's ratio. Research performed by Van Lier *et al.* [70] used ab initio calculations to define the mechanical properties of graphene. The results were in good agreement with the experimental and theoretical data. QM has also been used to investigate surface imperfections in graphene. Raskhit *et al.* [61] used DFT calculations to investigate the effects of ripples on the stress-strain behaviour .

Molecular dynamics Molecular dynamics (MD) is a technique to produce a dynamical trajectory of a system composed of N particles by integrating a potential function. MD uses either quantum mechanics, Newton's laws of motion, empirical data or a mixed model to define a potential function. The accuracy of the result of the simulation depends on the correct choice of potential function. An example of a potential used in graphene research is the Tersoff potential. The Tersoff potential is a many-body bond-order potential which means that the strength of a chemical bond depends on the bonding environment, including the number of bonds, angles and bond lengths. The energy is parameterised as the sum of a repulsive pair potentials and an attractive pairwise contribution that depends on the bond order. Long-range van der Waals interactions and bond-breaks are not taken into account. Other carbon potentials are Stillinger-Weber (SW) [27], REBO [12], AIREBO [67] and the EDIP potential [43]. Molecular dynamics has been implemented in different codes, for example in the open source Large-scale Atomic/Molecular Massively Parallel Simulator (LAMMPS) [56].

Molecular dynamics has been widely used to investigate the different properties of graphene. Zhang *et al.* [84] used MD simulations based on the AIREBO potential coupled with the Lennard-Jones potential to investigate the effects of layer number, temperature and isotope on the mechanical properties of graphene. Zhao *et al.* [86] investigated the size and chirality dependent elastic properties of graphene nanoribbons under uniaxial tension using MD simulations based on the AIREBO potential as well. Both results are in reasonable agreement with the experimental data. Gao *et al.* [21] and Lee [34] used the REBO potential to investigate rippling at finite temperature. Wrinkles have been investigated by Zhang *et al.* [83] using the REBO potential, were Min and Aluru [46] used the AIREBO potential. Although the Stillinger-Weber (SW) potential is not used often, the SW-potential is getting more attention as well. Especially in the case of mechanical deformation the SW-potential shows great potential [27].

Continuum modelling In continuum modelling (CM) only three sets of equations are of relevance: continuity, equilibrium and constitutive models. In dynamics the equilibrium equations are replaced by equations of motion. Although graphene is a membrane, membrane theory cannot be applied since membrane theory states that resistance to shear or bending forces can be neglected. However, experimental research showed that graphene has some bending rigidity [53]. Furthermore it was stated that the classic plate theory cannot be applied to define the bending rigidity of graphene as well, since the bending moduli of mono-layer graphene are not directly related to the in-plane Young's modulus and Poisson's ratio. The bending moduli of single layer graphene are resulting from interactions among the carbon atoms.

It is also questioned if assumptions to come up with the three sets of equations of classic continuum modelling hold for graphene. Especially the quantities like effective thickness and effective Young's modulus may not exist at the nanoscopic scale since classical continuum mechanics does not involve the atomic structure of graphene [73]. Therefore, different theories have been proposed which do include the small scale effects, often these theories are combinations of continuum modelling and atomistic modelling. An examples is nanoscale continuum modelling where the C-C bonds are replaced by continuum elements. Another example is the nonlocal elasticity theory, for which the stress tensor in a point depends on the deformation tensor in all other points of the entire domain of the material [18]. Also the modified couple stress theory [29] and modified strain gradient elasticity [31] can be used.

Arash *et al.* [6] showed that the classical elastic model overestimated the resonant frequencies of single-layered graphene sheets a lot. Sakhaee-Pour *et al.* [64] and Ansari *et al.* [4] applied non-local theories to investigate vibrations in single-layered graphene sheets. Their results were in good agreement with experimental work. Akgoz *et al.* [2] used the modified strain gradient theory and the modified couple stress theory to analyse the buckling behaviour of axially loaded micro-scaled beams. Their results were not in agreement with the results from classical continuum theory, but it could be that the classical continuum theory is not right. Wang *et al.* [73] investigated wrinkling in simply supported circular graphene under central point loading using continuum theory. Duan *et al.* [17] investigated the formation of wrinkles in single layer graphene sheets subjected to in-plane shear. Both assumed that bending rigidity and in-plane stiffness control the stiffness.

Course grained methods Course-grain (CG) methods are developed to improve continuum methods. In CG models small groups of atoms are treated as single particles. An example is shown in figure 2.8. Course-grain methods make it possible to simulate larger sizes or longer time scales than what is possible with classical mechanical potentials. Course-grained methods are often combined with other methods, so-called hybrid modelling techniques.

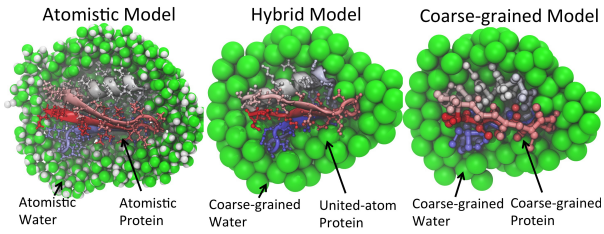

Figure 2.8: Representation of a protein at different levels of details. Image from [77].

An example is the atomic-scale finite element method (AFEM), developed by Liu *et al.* (2004). In AFEM the body is divided into atomic scale finite elements. Since every atom has a unit cell overlapping with the unit cell of the atom next to it, long- range interactions can be taken into account. Part of the structure can be modelled with classic FEM and part can be modelled using AFEM. Transitional elements ensure the smooth transition between AFEM and continuum FEM elements [36]. Another example is the course-grained MD were each bead represents four atoms of the graphene atomistic lattice.

Liu *et al.* [36] used AFEM to investigate vibration frequencies in carbon nanotubes. Wang and Guo [75] used the quantum continuum method to model the deformation of single layer graphene sheets. Both results were in good agreement with previous work.

Comparison of modelling techniques Quantum mechanics-based methods are considered as the most accurate among all computational techniques. Especially DFT is widely used for graphene simulations. Their applications are however limited to small systems, because of the high computational costs and the time length of the simulations.

Molecular dynamics is a strong research method, and has been used often for research into graphene. The strength of molecular dynamics lies in its accuracy: with the correct potential field, complex systems can be accurately modelled. Interatomic potentials often have been used to describe the mechanical behaviour of nanoscale materials. Furthermore, if the right potential is chosen, the computation can be very efficient.

Course-grained methods combine accuracy and computational efficiency. However, since these methods have not been used to model surface imperfections, it is hard to say if the results will be accurate. These methods although show good potential.

Different types of continuum modelling are used for the analysis of the mechanical properties of graphene. Classical continuum modelling is computational efficient and easy to use, however the validity is limited. Higher order continuum models are more accurate, however complicated equations are needed and they are not practical. Furthermore, higher order continuum models are still in development for graphene.

2.4. Conclusions

Graphene exhibits some exceptional properties in different areas of interest. Although a lot of research has already been performed, it was shown that a spread in theoretical predictions of the different properties still exists. It was stated that imperfections are inevitably in bulk production techniques. Therefore it is important to know the effects of imperfections on the different mechanical properties of graphene. It was stated that all types of structural imperfections without foreign atoms will result in a reduction of the elastic modulus, failure strain and intrinsic strength. Depending on the density of the defects the reduction can be more severe. The effects of finite temperature and therefore the effects of rippling on the elastic properties have not been fully established. Also, the effect of the amount of stress on the wrinkle amplitude is questioned. Although literature does agree on the softening effect of wrinkling, crumpling and rippling, the contribution of wrinkling to the softening behaviour of crumpled graphene have only been investigated experimentally on circular membranes. Also, research showed that the thermal expansion coefficient is determined by the rippling behaviour, the effect of wrinkles is not investigated. Moreover, the effect of wrinkles on the bending rigidity has not been established yet. At last, literature showed that ripples and wrinkles can induce the positive Poisson's ratio to become negative. Three types of modelling techniques were discussed, continuum modelling, atomistic modelling and coarse-grained modelling. It was stated that all types could be used to investigate the mechanical properties of graphene and the effects of surface imperfections in graphene. Based on the review, molecular dynamics based on empirical potentials shows great potential to model surface imperfections in graphene. Furthermore, to compare these results the continuum approach could be used.

To summarise, the following relevant research gaps were identified:

- To study the mechanical properties of graphene to decrease the spread in theoretical predictions.
- To find possibilities to improve the bulk production techniques of graphene.
- To study the effects of finite temperature and therefore the effects of rippling on the elastic properties of single layer graphene.
- To investigate the effect of the amount of stress on the wrinkle amplitude.
- To investigate the contribution of wrinkling to the softening behaviour of crumpled graphene on non-circular membranes.
- To investigate the effect of wrinkling on the thermal expansion coefficient of graphene.
- To study the effect of wrinkles on the bending rigidity of graphene membranes.
- To incorporate surface imperfections in coarse-grained models of graphene membranes.

3

Research question, objectives and research methodology

3.1. Research objectives and questions

As presented in chapter 2, the current state of research, concerning imperfections in graphene, is still at an early stage. Recent experimental studies have shown significant effects of wrinkles on the mechanical properties of graphene, both in singly and doubly clamped graphene beams. In fact, static wrinkles, with apparent heights up to 30 nm, are large enough to influence the mechanical response of graphene membranes. Although the obvious significance of understanding the effects of imperfections on the properties of graphene, both for fundamental understanding as well as applications, the effects have not been understood thoroughly. These observations bring a need for a broader investigation around the formation of static wrinkles and their effects on the mechanical response of single layer graphene both singly and doubly clamped. Furthermore, it is recognised that both continuum modelling and molecular dynamics simulations provide suitable modelling approaches for the analysis of surface imperfections in graphene, and therefore it is proposed to use these modelling techniques when studying wrinkled graphene membranes. Based on the posed demand, this research studies the effects of wrinkles on the mechanical properties of single layer graphene membranes, by making use of both continuum model modelling and molecular dynamics simulations.

In summary, the objective of this research is to contribute to the understanding of the mechanics of single layered graphene membranes with surface imperfections by making use of molecular dynamics modelling as well as continuum modelling.

To reach this objective, answers will be sought to two main research questions:

- Could a constitutive model be established to describe the mechanical behaviour of wrinkled rectangular ribbons of graphene during the transition from the wrinkled state to the flat state, based on the simulation results obtained in both molecular dynamics and continuum mechanics?
- Could a graphene nanocantilever, modelled in molecular dynamics, be stabilised by wrinkles?

3.2. Research methodology

In this study, we develop a model to predict the mechanical response of wrinkled single layer graphene ribbons during the transition from the wrinkled state to the flat state as well as a model to stabilise a single layer graphene cantilever. For this purpose, first, we build an atomistic model of a wrinkled single layer graphene nanoribbon and a wrinkled nanocantilever in the molecular dynamics (MD) software LAMMPS and a continuum model of the equivalents in the FEM software COMSOL. To investigate the mechanical response of ribbons, these wrinkled ribbons are stretched equibiaxially to obtain the non-homogenous stress-strain response. Next to the MD simulations, a deterministic microstructure description is developed to describe the wrinkled layers. The data obtained from the MD simulations and the set of microstructure descriptors are used to fit a constitutive model. To investigate the stabilisation of nanocantilevers by implying a curvature, layers with varying aspect ratios and different rates of curvature are modelled in molecular dynamics.

II

Papers

4

Paper: Comments on the hidden area of nonlinearity in graphene

Comments on the hidden area of nonlinearity in graphene

Laura Dijkink,[1,*] Farbod Alijani,[1] Banafsheh Sajadi,[1] and Peter G. Steeneken[1,2]

[1] *Department of Precision and Microsystem Engineering, Delft University of Technology, 2628 CD Delft, The Netherlands*

[2] *Kavli Institute of Nanoscience, Delft University of Technology, 2628 CJ Delft, The Netherlands*[†]

(Dated: January 29, 2019)

A new constitutive model, an exponential extension of Hooke's law, was recently proposed by Grima *et al.* [1] and used by Nicholl *et al.* [2] to approximate the behaviour of crumpled graphene membranes during stretching. It was shown that this exponential Hooke's law is capable of describing the nonlinearity at small strains in wrinkled graphene by an unique exponent of 0.1. Here we show, by applying equibiaxial tension in molecular dynamics simulations of wrinkled single layer graphene sheets, that this exponent is not unique but rather varies between $0.5 - 1.0$. It is demonstrated that the model fails to predict the nonlinear response during flattening of wrinkled graphene membranes with an average out-of-plane displacement of the atoms between 0.5 Å and 2.71 Å. Instead, we show that Ogden's well accepted constitutive law in nonlinear elasticity can be very well used to capture the nonlinearity in the mechanical behaviour during flattening of wrinkled membranes irrespective of the average out-of-plane displacement. Furthermore, Ogden's law provides insights into the shear modulus and, already predicted, negative Poisson's ratio of wrinkled graphene. This study demonstrated that the Poisson's ratio of wrinkled graphene membranes varies between -0.9 and 0.16 and the shear modulus between 4950 GPa and 270 GPa during stretching between 0 % and 15 % strain.

Keywords: Graphene; Static Wrinkles; Constitutive models; Nonlinear identification; Poisson's ratio; Shear modulus

INTRODUCTION

The outstanding mechanical properties of graphene have made it a suitable candidate for a wide range of sensor and actuator applications in modern technology, such as ultra-capacitors [3, 4] and solar cells [5]. However, before the full potential of future applications can be achieved, a proper characterisation of the fundamental properties of graphene membranes is crucial. It has been shown that graphene membranes are inherently wrinkled and rippled. Although one might be concerned that the presence of surface imperfections will affect the mechanical properties to the extent that it would become unusable in practical applications, research showed that for some applications imperfections are useful. It seems that for batteries and super capacitor applications highly imperfect graphene is even preferred [6]. In addition, researchers are currently exploring the possibility on scavenging vibrational energy from surface corrugations as alternative to batteries [7].

The mechanical properties of graphene have been extensively studied. Theoretical and experimental studies predicted a Young's modulus of 1 TPa [8, 9]. Lower values have been obtained in experimental studies since manufactured samples often have imperfections in contrast to theoretical studies. Research showed that structural defects result in a lower Young's modulus, failure strain and intrinsic strength [10–15]. From theory it was predicted that atomic mismatches could also induce wrinkles [16]. Nonlinear behaviour at small strains caused by these defect induced wrinkles was demonstrated by different studies [1, 17]. Besides wrinkles, thermal fluctuations occur intrinsically in graphene, resulting in ripples. Intrinsic ripples induce nonlinear stress-strain behaviour at small strains [18–21], a higher bending rigidity [22, 23] and a lower Young's modulus [19, 24]. In fact, static wrinkles, with apparent heights up to 30 nm, and ripples with heights around the layer thickness, are large enough to influence the mechanical response of suspended graphene membranes.

Different constitutive models have been proposed to describe the stress-strain relation of graphene. Lee *et al.* [25] proposed a second order Taylor series in power of strain, where the nonlinearity is expressed by a third-order elastic modulus D. Cadelano *et al.* [26] noted that, despite the fact that D summarises the nonlinear features, continuum elasticity predicts three independent third-order parameters. Therefore a constitutive law including three independent third-order parameters was developed. Wei *et al.* [27] stated that this description is however unable to reflect both the response at infinitesimal strain and finite strain, which led to the development of a fifth order nonlinear continuum description. Although these models all obtain a certain numerical accuracy, they fail to attribute the characteristics to the underlying material physics of the layer. Recently a model has been proposed that does capture the underlying material physics. Gornyi *et al.* [28] proposed a constitutive law to describe the transition from the nonlinear response, caused by wrinkles and ripples, to the linear response. One objective of this work is to investigate different constitutive models to describe the nonlinear stress-strain relation attributed to static surface imperfections in single-layer graphene membranes.

To investigate the effects of wrinkles, different modelling techniques have been used. Experimental studies often use indentation techniques, however, this can change the amplitudes of the corrugations. Furthermore, it is hard to make a distinction between the effects of the ripples and wrinkles since experiments are often performed at room temperature. Using molecular dynamics (MD) simulations it is possible to exclusively study the effects of wrinkles in pristine graphene. Therefore, the other objective of this work is to develop a MD model to investigate the transformation of single layer graphene from the wrinkled state to the flat state.

ATOMISTIC SIMULATIONS

Molecular dynamics simulations were performed using the large-scale atomic/molecular massively parallel simulator (LAMMPS) software [29]. A pristine single layer of graphene consisting of a total of 3854 carbon atoms with a size of 100 Å by 100 Å was formed. This size is large enough to ignore the size effect of graphene [30]. Periodic boundary conditions were applied. Accuracy of the results strongly depends on the correct choice of potential function. In our study, the atomic interactions were defined by the Tersoff potential [31], which has shown considerable validity in the evaluation of the mechanical properties of single layer graphene [13, 32]. It must be noted that long-range interactions are not taken into account using Tersoff potential, like AIREBO [33] and REBO [34] do. Since our work was only dealing with single layer graphene it was not needed to include these long-range interactions. A time step of 1 fs was used. The system was thermalized in the NVT ensemble at 1 K with the right boundary fixed in the x-, y- and z-direction, the left boundary fixed in the z-direction and the other boundaries free to move, to make sure that no internal stresses were build up during thermalization. After thermalization the wrinkled structure was created by applying a parametrized shear at the left boundary in the NPT ensemble at zero pressure. The shear was applied for 0.05 ns after which the system was relaxed for 0.5 ns. After the wrinkled structure was formed, the system was stretched equibiaxially at a constant strain-rate of 0.0005 Å/fs. The strain was applied for 0.5 ns after which the system was relaxed for the same amount of time. This strain-increment was applied 40 times, so the layer was stretched 10 Å in all directions, which corresponds to 20 % strain. The engineering stresses were obtained by calculating the forces at the boundaries.

Experimental research indicated that different wrinkling patterns can occur in suspended graphene sheets. Wrinkled regions are often consisting of consecutive formations of folds of which the amplitude gradually increase along the length of the layer. Multiple wrinkled regions with different wrinkling patterns can exist in one layer, an example is shown in figure 6a. Fifteen different wrinkling pattern are investigated created by five different parametrized boundary conditions with three different magnitudes. The different parametrized boundary conditions result in different wrinkling configurations according to length, amplitude, orientation and number of wrinkles. Two of the fifteen samples can be seen in figure 6b and 6c. An overview of the fifteen different wrinkled ribbons can be seen in S1.

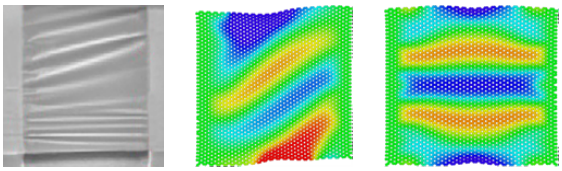

FIG. 1: Wrinkles in graphene membranes. a) Wrinkles seen in a real graphene layer. Image from [35], courtesy of A. K. Geim and C. N. Lau, respectively. b) and c) Two of the investigated samples. Colours indicate out-of-plane displacement. Results visualised with [36].

MECHANICAL RESPONSE OF WRINKLED GRAPHENE UNDER EQUIBIAXIAL TENSION

A typical stress-strain response of a wrinkled graphene ribbon at 1 K under equibiaxial tension is displayed in figure 2a. The stress-strain curve is obtained by averaging the nominal stresses working on the boundaries. The retrieved curve is divided into three parts. Part I, between 0 % and ∼1 % strain, is the soft nonlinear part. The simulations were performed at low temperatures to cancel out the effect of dynamic ripples caused by thermal fluctuations. Doing as such, the nonlinear mechanics at low strains can be fully attributed to the presence of wrinkles. This part thus captures the transition from the wrinkled state to the flat state. At the start, this first part is dominated by stretching of the wrinkles after which stretching of the bonds starts as well, which causes an increase in the stress-strain slope. The average out-of-plane displacement is decreasing in this part, displayed in figure 2b. In the second region, between ∼1 % and ∼5 % strain, the slope is linear, this second part is dominated by stretching of the bonds resulting in a nearly constant out-of-plane displacement of the layer. In the last part, after ∼5 % of strain, the graphene bonds are stretched beyond the limit and bonds will eventually break. The coming parts of this paper focus on the mechanical behaviour at small strains, part I and part II, since the nonlinear behaviour caused by wrinkling is dominant in these parts.

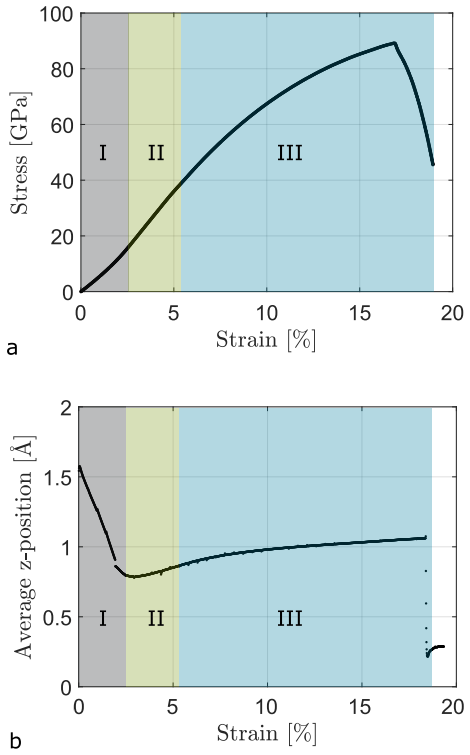

FIG. 2: Stretching of a wrinkled graphene layer. Part I: Nonlinear part, dominated by stretching of the wrinkles. Part II: Linear part, dominated by stretching of the bonds. Part III: Nonlinear part, yield and failure. a) Typical stress-strain curve of a wrinkled layer of graphene. b) Average z-position of atoms of a wrinkled layer of graphene.

NONLINEAR MECHANICS EXPLAINED BY DIFFERENT CONSTITUTIVE MODELS

To further investigate and quantify the nonlinear behaviour at small strains different models can be used. Recently an exponential Hooke's law was presented by Gornyi *et al.* [28] and used by Nicholl *et al.* [2] to approximate the behaviour of crumpled graphene membranes during stretching, using the following equation:

$$\epsilon(\sigma) = \frac{\sigma_*}{E_{2D}}\left[\frac{\sigma}{\sigma_*} + \frac{1}{\alpha}\left(\frac{\sigma}{\sigma_*}\right)^{\alpha}\right] \tag{1}$$

The equation consists of two parts, the first part is the linear part, which describes the stretching of the carbon-carbon bonds, corresponding with part II of figure 2. The second part is the nonlinear part, describing part I of figure 2, in which the nonlinearity is determined by α. The transition point, at which bond-stretching is dominant over flattening of the surface roughness, is determined by σ_*.

This exponential Hooke's law was fitted to the data at small strains obtained from MD. Typical results can be seen in figure 3a and 3d. According to [28] and [2], α should be ~ 0.1 for wrinkled membranes, irrespective of the amount of wrinkling. We fitted our data from the MD simulations to equation 1, were α and σ_* are the fitting parameters. E_{2D} is set to 1029 GPa [8]. The nonlinearity exponent α was found to vary between $0.5 - 1.0$ for different wrinkle patterns, which does not agree with what has been predicted experimentally. The cross-over stress was found to vary between 0 GPa and 1.01 GPa (S3). To verify the values obtained for the cross-over stresses from the fitting to equation 1, the values are compared to the turning points from MD. The numerically obtained turning points are the points at which the slope of the stress-strain curve becomes linear, corresponding to the start of part II of figure 2. These turning points are between 5.45 GPa and 12.53 GPa. It was noticed that the cross-over stresses predicted by the fitting of equation 1 are not agreeing with the values from molecular dynamics. The presented exponential Hooke's law is underestimating the cross-over stress. By taking a closer look at the values for σ_* it appears that these stresses are the first changes of the slopes of the stress-strain curves. From all this, it is concluded that the presented exponential Hooke's law fails to describe the transition from the wrinkled state to the flat state accurately.

Another way of representing nonlinear behaviour of elastic systems is by strain energy density functions depending on the right Cauchy-Green deformation tensor or Green's strain tensor [37]. Different strain energy density functions have been developed to describe the hyperelastic softening behaviour seen in wrinkled graphene. We have tested different models in order to determine the model that characterises the nonlinear behaviour the best, as can be seen in supplementary material 2. We found that Ogden's law is well-suited for representing the nonlinear behaviour at small strains.

The Ogden's law was introduced in 1972 [38]. The strain energy density function for a compressible isotropic Ogden material can be expressed in terms of the principal stretches $\lambda_1, \lambda_2, \lambda_3$. The principal stretches can be obtained from the normal strains, ϵ_i, using $\lambda_i = \epsilon_i + 1$. The strain energy density function is then defined by:

$$W(\lambda_1, \lambda_2, \lambda_3) = \sum_{i=1}^{N} \frac{\mu_i}{\alpha_i}(\lambda_1^{\alpha_i} + \lambda_2^{\alpha_i} + \lambda_3^{\alpha_i} - 3) + f(\lambda_1, \lambda_2, \lambda_3), \tag{2}$$

where N denotes the order of the model, α_i and μ_i are fitting parameters and f is the volumetric part of the model. In this model α_i and μ_i must satisfy the requirement

$$\sum_{i=1}^{N} \mu_i \alpha_i = 2\mu, \tag{3}$$

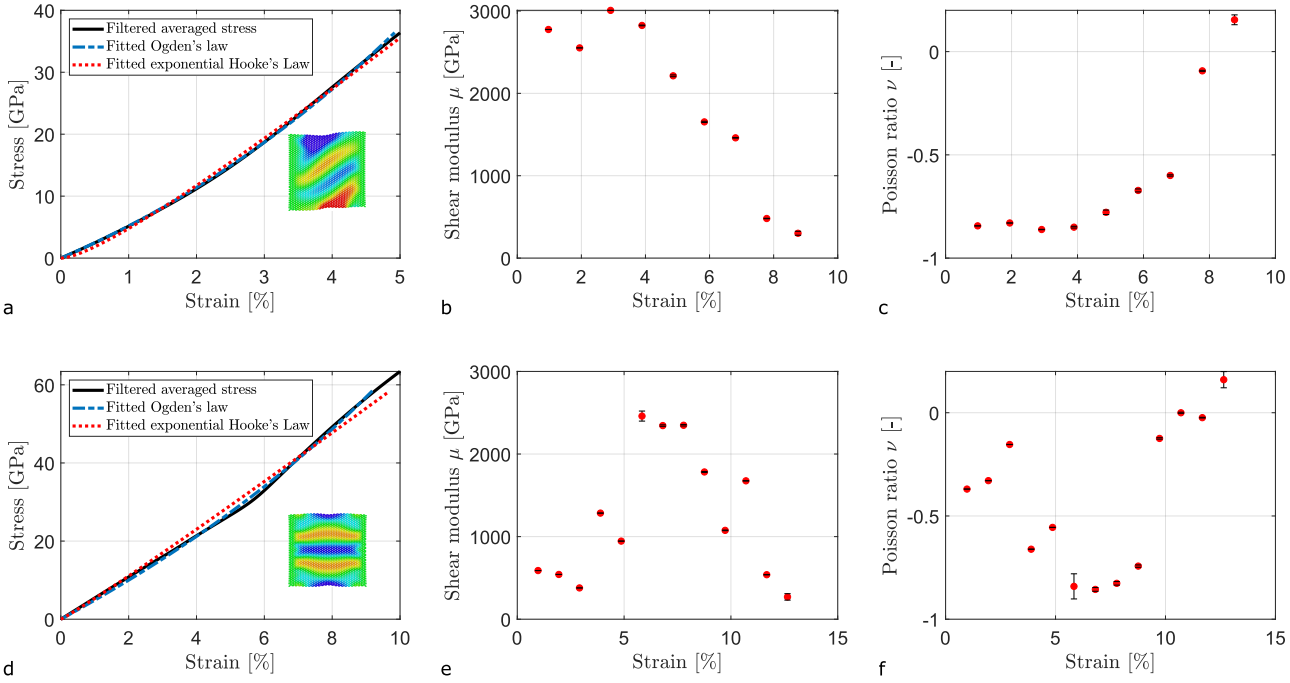

FIG. 3: Mechanical response of two wrinkled graphene membranes. a) and d) Filtered averaged stress obtained in MD during equibiaxial tension, exponential Hooke's law (red) as well as first order Ogden law (blue) are fitted for 0 %-5 % and 0 %-10 % strain. b) and e) Shear modulus during stretching. c) and f changing Poisson's ratio during stretching. Vertical lines indicate the proportional squared sum of residuals.

where μ is the shear modulus of the material in the undeformed stress-free configuration. The volumetric part of the Ogden model in equation 2 can be expressed as

$$f(\lambda_1, \lambda_2, \lambda_3) = \sum_{i=1}^{N} \frac{\mu}{\alpha_i} \frac{1}{n} \left(J^{-n\alpha_i} - 1 \right), \tag{4}$$

where $J = \lambda_1\lambda_2\lambda_3$ and n is given by [39]

$$n = \frac{\nu}{1 - 2\nu}, \tag{5}$$

where ν is the Poisson's ratio. Under the assumption of isotropy $\sigma_1 = \sigma_2$ and $\sigma_3 = 0$, and equibiaxial tension, $\lambda_1{=}\lambda_2{=}\lambda$, λ_3 is given by $\lambda_3 = \lambda_1^{\frac{-2n}{n+1}}$ [40]. The first order Ogden model in terms of nominal stresses, S, and principal stretches, λ, then reduces to,

$$S = \sum_{i=1}^{N} \mu_i \left(\lambda^{\alpha_i - 1} - \lambda^{\frac{-2n\alpha_i}{n+1} - 1} \right). \tag{6}$$

This Ogden's law was fitted to the small strain data extracted from MD. The fittings obtained were really good with an squared sum of residuals between $0.0026 - 4.33$ (S3). Typical results can be seen in figure 3a and figure 3d.

It was already stated that α_1 and μ_1 must satisfy the requirement of equation 3. From the fitting of Ogden's law to the stress-strain data of a non-wrinkled layer from MD it comes clear that this requirement holds for our ribbon. To investigate the shear modulus in more detail the requirement of equation 3 was used. Ogden's law was fitted for different strain rates, from which the shear modulus was obtained for the different strain rates, as can be seen in figure 3b and 3e. It can be seen that the shear modulus is decreasing after flattening of the membrane. For all fifteen samples the shear modulus between 0 % and 1 % strain was found to vary between 200 GPa for almost flat layers up to 4950 GPa for wrinkled layers, as can be seen in figure 4.

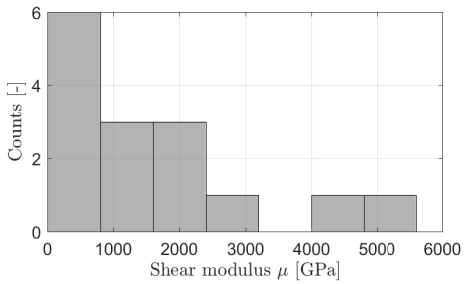

FIG. 4: Histogram of the obtained shear modulus μ for all samples between 0 % and 0.97 % strain.

The shear modulus for flat graphene mentioned in literature is between 213 GPa and 450 GPa [41, 42]. It is observed that the shear modulus obtained for the wrinkled ribbons of this research are up to a factor 10 higher. This could be explained by the fact that the wrinkles are created by applying a shear stress at the boundaries. This will result in a residual stress in the boundaries and therefore result in a larger shear modulus, according to the definition of the shear modulus.

Ogden's law also provides insights into the Poisson's ratio, according to equation 5. To investigate the Poisson's ratio in more detail, ν was obtained for different strain rates. In figure 3c and 3f typical responses of the Poisson's ratio under increasing strain can be seen. The Poisson's ratio is initially negative, after flattening it gradually increases when the strain is increased. At a certain point the Poisson's ratio turns positive up to 0.16, which corresponds with the Poisson's ratio found for flat graphene. Furthermore, for the different samples ν was found to vary between -0.9 and 0.16 for a strain-rate between 0 % and 1 %, as can be seen in figure 5.

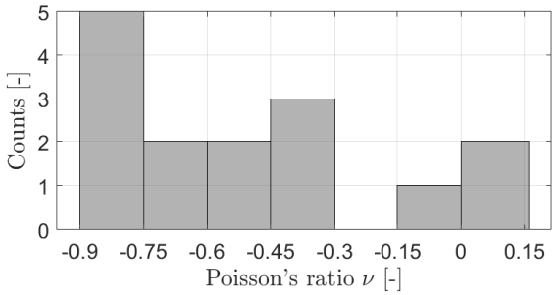

FIG. 5: Histogram of the obtained Poisson's ratio ν for all samples between 0 % and 0.97 % strain.

Several authors already predicted the presence of a negative Poisson's ratio in corrugated graphene membranes [1, 17, 43]. In these works corrugated graphene was stretched uniaxially, the corresponding contraction or expansion in the other direction was measured. Using linear Hooke's law the Poisson's ratio was determined according to $\nu = -\frac{\epsilon_{yy}}{\epsilon_{xx}}$. According to our results it is by definition incorrect to determine the Poisson's ratio based on linear Hooke's law, since corrugated graphene exhibits nonlinear behaviour. Using a constitutive law capable of incorporating this nonlinear behaviour, for example Ogden's law, is preferred.

CONCLUSION

In conclusion, we report on the transition due to stretching from nonlinear behaviour at small strains to the linear response at higher strain rates of wrinkled graphene membranes. We were able to simulate this transition for different initial wrinkling configurations using atomistic modelling techniques. Different constitutive laws have been investigated to describe the mechanical response. It was concluded that the presented exponential Hooke's law failed to reproduce the nonlinearity at small strains correctly. The nonlinearity at small strains is well described by the first order compressible Ogden's law. Ogden's law predicted a negative Poisson's ratio at small strains for wrinkled membranes, which is in agreement with previous research. Also, Ogden's law predicted a decreasing shear modulus and an increasing Poisson's ratio after flattening. In addition, this research showed that the mechanical properties of graphene could be tailored by implying wrinkles. Tailoring the mechanical properties of graphene in an experimental setting is an interesting field for future research.

SUPPLEMENTARY INFORMATION: COMMENTS ON THE HIDDEN AREA OF NONLINEARITY IN GRAPHENE

S1 presents the fifteen different samples investigated in this research. Section S2 gives an overview of the fitting of different hyperelastic constitutive laws. In section S3, we show the complete datasets obtained of the fitting of the exponential Hooke's law and Ogden's law to the stress-strain data from MD. In section S4 the nonlinear mechanical behaviour of the wrinkled membranes is compared with the mechanical behaviour of crumpled and rippled membranes. Movie 1 shows the formation of wrinkles by displacing the boundaries. Movie 2 shows stretching of a wrinkled membrane.

S1: OVERVIEW OF THE INVESTIGATED SAMPLES

Fifteen different samples are investigated in this research, which can be seen in figure 6. By displacing the boundaries in a certain direction the different wrinkled membranes were created, as can be seen in movie 1. The samples are described with five different corrugation descriptors, as can be seen in table I.

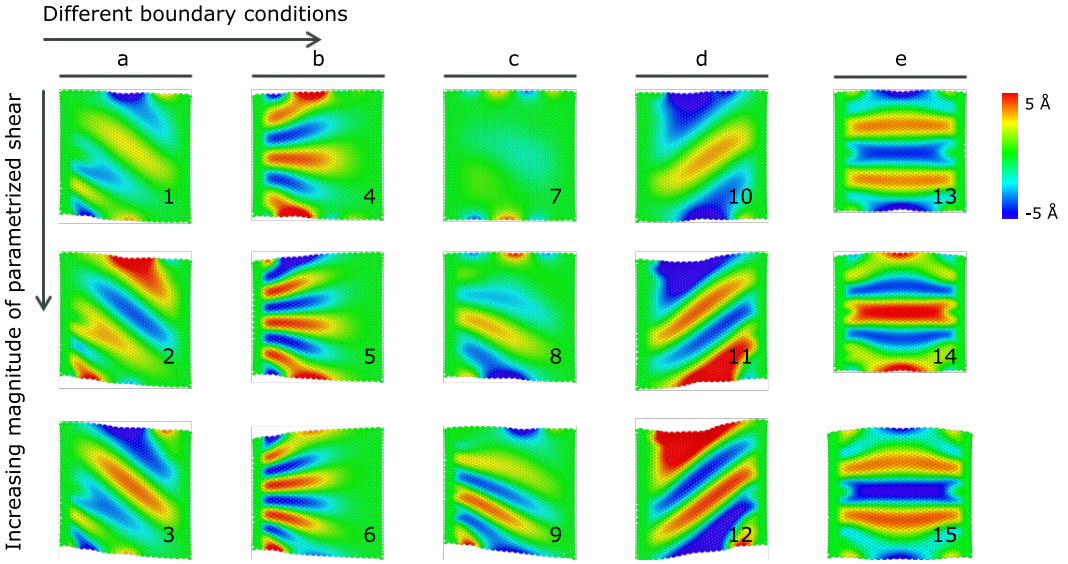

FIG. 6: The investigated samples. The letters correspond with the five different parametrized boundary conditions. Colours indicate out-of-plane displacement. Results visualised with [36].

TABLE I: Values of the corrugation descriptors for all samples.

	1	**2**	**3**	**4**	**5**	**6**	**7**	**8**	**9**	**10**	**11**	**12**	**13**	**14**	**15**
Volume/area	1,09	1,46	1,51	0,85	0,95	0,79	0,21	1,11	1,25	1,78	1,99	2,49	1,92	1,97	1,95
Average out-of-plane displacement	1,14	1,53	1,59	0,87	0,92	0,81	0,50	1,14	1,27	1,83	2,04	2,71	1,92	1,95	1,93
Total number of wrinkles	3,00	3,00	3,00	3,00	4,00	5,00	4,00	4,00	4,00	2,00	3,00	3,00	3,00	3,00	3,00
Average wrinkle height	2,28	6,89	2,80	4,75	3,36	3,85	3,50	3,04	5,63	1,57	3,00	7,91	1,29	6,26	3,60
Average orientation angle of the wrinkles	-21,58	-23,93	-27,10	1,36	-2,35	-1,01	-6,77	-7,94	-10,22	19,83	15,23	23,55	-0,14	-0,25	0,11

S2: FITTING OF DIFFERENT HYPERELASTIC CONSTITUTIVE LAWS

To investigate the nonlinear response in more detail hyperelastic models can be used. In this section an analysis is performed of the fitting of different compressible isotropic hyperelastic constitutive laws to the data obtained from MD. The hyperelastic laws considered are the neo-Hookean, Mooney-Rivlin and Ogden:

- Neo-Hookean:

$$W = C_1(\overline{I_1} - 3) + D_1(J-1)^2 \tag{7}$$
$$\overline{I_1} = J^{(-2/3)} I_1. \tag{8}$$

- Mooney-Rivlin:

$$W = C_{10}(I_1 - 3) + C_{01}(I_2 - 1) + C_{11}(I_1 - 3) + C_20(I_1 - 3)^2 + \cdots + D(J-1)^2 \tag{9}$$

- Ogden:

$$W(\lambda_1, \lambda_2, \lambda_3) = \sum_{i=1}^{N} \frac{\mu}{\alpha_i} \left(\lambda_1^{\alpha_i} + \lambda_2^{\alpha_i} + \lambda_3^{\alpha_i} - 3\right) + f\left(\lambda_1, \lambda_2, \lambda_3\right), \tag{10}$$

where N denotes the order of the model, α_i and μ_i are fitting parameters and f is the volumetric part of the model. The volumetric part of the Ogden model can be expressed as

$$f(\lambda_1, \lambda_2, \lambda_3) = \sum_{i=1}^{N} \frac{\mu}{\alpha_i} \frac{1}{n} (J^{-n\alpha_i} - 1), \tag{11}$$

where n is a material constant related to the Poisson's ratio according to $n = \frac{\nu}{1-nu}$ [39].

These hyperelastic functions are given in terms of invariants of the right Cauchy-Green strain tensor, I_1, I_2, I_3, and principal stretches, λ_1, λ_2,λ_3. The expressions of these invariants in terms of principal stretches are derived from the Green-Lagrange strain tensor:

$$\mathbf{E} = \frac{1}{2} \begin{pmatrix} 2\epsilon_1 & \epsilon_{12} & 0 \\ \epsilon_{12} & 2\epsilon_2 & 0 \\ 0 & 0 & 2\epsilon_3 \end{pmatrix} \tag{12}$$

The right Cauchy-Green strain tensor $\mathbf{C}$ is then given by:

$$\mathbf{C} = 2\mathbf{E} + \mathbf{I} = \begin{pmatrix} 2\epsilon_1 + 1 & \epsilon_{12} & 0 \\ \epsilon_{12} & 2\epsilon_2 + 1 & 0 \\ 0 & 0 & 2\epsilon_3 + 1 \end{pmatrix} \tag{13}$$

Small strains are assumed, therefore the displacements can be expressed in terms of the principal stretches according to $\lambda = \epsilon + 1$. Resulting in the following three invariants:

$$I_1 = \text{tr } \mathbf{C} = \lambda_1^2 + \lambda_2^2 + \lambda_3^2 \tag{14}$$
$$I_2 = \frac{1}{2}\left(\text{tr } \mathbf{C}^2 - \text{tr } (\mathbf{C})^2\right) = \lambda_1^2\lambda_2^2 + \lambda_2^2\lambda_3^2 + \lambda_1^2\lambda_3^2 \tag{15}$$
$$I_3 = J^2 = |\mathbf{C}| = \lambda_1^2\lambda_2^2\lambda_3^2 \tag{16}$$

In case of an incompressible material J is used to reflect the incompressibility using $J = 1$. In our work the material is assumed to be compressible. From Ogden's law an expression for J can be extracted. In the case of equibiaxial tension the following holds: $S_1 = S_2, S_3 = 0$, and $\lambda_1 = \lambda_2 = \lambda$. From this, λ_3 is extracted [40]: $\lambda_3 = \lambda_1^{\frac{-2n}{n+1}}$. Resulting in the following expression for J:

$$J = \lambda_1\lambda_2\lambda_3 = \lambda^{\frac{2}{n+1}} \tag{17}$$

This J denotes the compressibility of the material and is used in the expressions of neo-Hookean, Mooney Rivlin and Ogden.

Using these expressions the hyperelastic models in case of equibiaxial tension are expressed in terms of nominal stresses, S, and principal stretches, λ:

- Generalised neo-Hookean

$$S_1 = S_2 = \frac{\mu}{J^5/3}\left(\lambda - \frac{J^2}{\lambda^5}\right) \tag{18}$$

$$S_3 = 0 \tag{19}$$

- Generalised Mooney-Rivlin
  Example of expression of Mooney-Rivlin model:

$$S_1 = S_2 = 2C_{10}\left(\lambda - \frac{J^2}{\lambda^5}\right) \tag{20}$$

$$S_3 = 0 \tag{21}$$

  By including more terms the fitting will become more accurate. The models included in this research can be seen in table II.

TABLE II: Mooney-Rivlin material models included in this research

Mooney-Rivlin 1	Mooney-Rivlin 2	Mooney-Rivlin 3	Mooney-Rivlin 4
C_{10}	C_{20}	C_{20}, C_{01}	C_{10}, C_{20}

- Generalised Ogden

$$S_1 = S_2 = \sum_{i=1}^{N} \mu_i \left(\lambda^{\alpha-1} - J^{-\alpha n-1}\right) \tag{22}$$

The resulting fittings to the stress-strain data obtained from MD can be seen in figure 7, also the sum of squared errors (SSE) are shown. It can be seen that the errors for the Ogden model as well as the fourth Mooney-Rivlin model are low. Furthermore it can be seen that increasing the order of the Ogden model does not improve the fitting.

As already has been said, the Mooney-Rivlin model is more or less a curve-fitting tool and does not provide any information about the mechanical properties. The Ogden model however does give insights into the mechanical properties of the membrane. In combination with the low error it was therefore decided to use the first order Ogden's law to represent the nonlinear behaviour of wrinkled graphene at small strains.

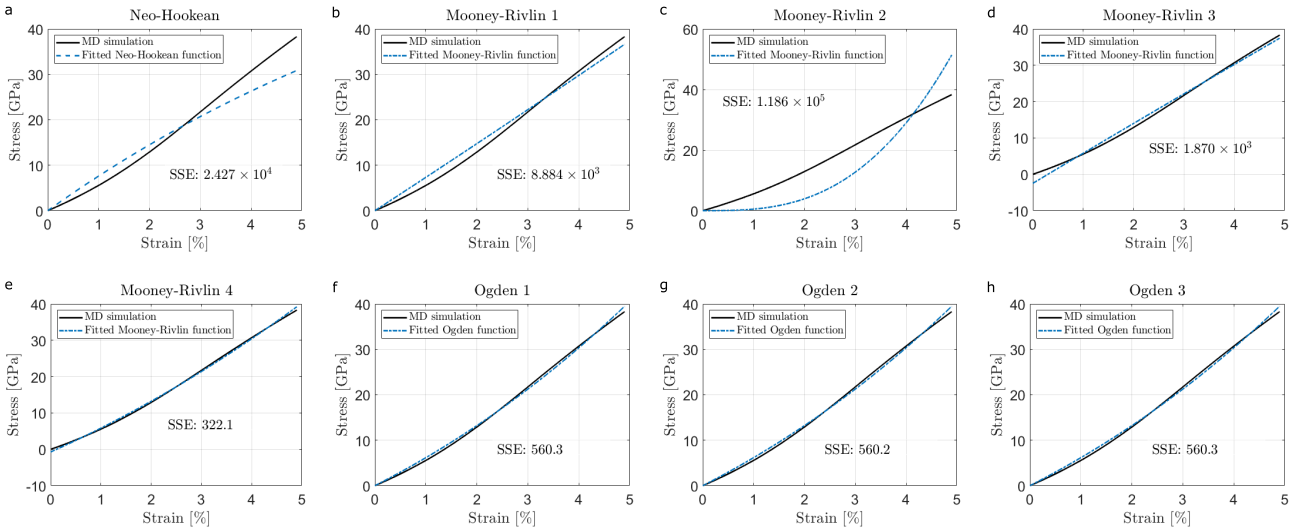

FIG. 7: a-g show the fitting of different constitutive laws to the stress-strain data obtained in MD simulations. The sum of squared errors (SSE) is showed as well.

S2: COMPLETE RESULTS OF FITTING EXPONENTIAL HOOKE'S LAW AND OGDEN'S LAW

In this section the fitting parameters as well as the fittings itself of the fifteen investigated samples are presented. In table III the results from fitting of the exponential Hooke's law are presented. In table IV the fitting parameters from the fitting of the first order Ogden's law are presented. Figures 8a-d, figures 9a-d, figures 10a-d and figures 11a-c show the actual fitting of the exponential Hooke's law and Ogden's law to the filtered averaged stress data obtained from MD. Figures 8e-h, figures 9e-h, figures 10e-h and figures 11d-f show the shear modulus obtained from fitting Ogden's law at different strain-rates. Figures 8i-l, figures 9i-l, figures 10i-l and figures 11g-i show the Poisson's ratio obtained from fitting Ogden's law at different strain-rates.

TABLE III: Obtained values for the fitting parameters of the exponential Hooke's law and the numerically obtained turning point analysis.

	1	**2**	**3**	**4**	**5**	**6**	**7**	**8**	**9**	**10**	**11**	**12**	**13**	**14**	**15**
σ_* **[GPa]**	0,56	1,34	1,68	0,06	0,00	0,00	0,00	0,40	0,55	0,00	1,67	0,00	1,000	1,000	1,000
α **[-]**	0,52	0,58	0,63	0,70	0,95	0,94	0,50	0,49	0,73	0,87	0,53	1,01	0,885245	0,953808	0,97111
Stress at turning points [GPa]	9,31	7,96	7,60	10,20	8,96	9,09	12,53	9,83	8,35	11,27	13,67	5,45	30,29	34,76	36,71
Squared sum of residuals	1.9×10^{-4}	5.6×10^{-4}	8.4×10^{-4}	6.3×10^{-5}	1.5×10^{-4}	1.2×10^{-3}	3.2×10^{-3}	1.7×10^{-4}	6.8×10^{-5}	8.9×10^{-5}	1.4×10^{-3}	2.3×10^{-3}	0.028 586	0,017749	0,011331

TABLE IV: Obtained values of the fitting parameters of Ogden's law

	1	**2**	**3**	**4**	**5**	**6**	**7**	**8**	**9**	**10**	**11**	**12**	**13**	**14**	**15**
μ **[-]**	470,46	497,41	512,65	528,17	645,54	110576,87	425363,5962	492,63	500,57	611,20	497,01	535,51	28,40171	38,00406	48,30004
α **[-]**	17,69	10,08	6,03	5,52	2,82	0,01	0,001948429	13,98	8,83	3,54	10,27	6,66	12,18565	9,181357	7,431042
n **[-]**	-0,32	-0,31	-0,29	-0,27	-0,23	0,18	0,227720702	-0,31	-0,30	-0,23	-0,31	-0,31	0,23	0,23	0,23
Squared sum of residuals	7.9×10^{-2}	3.36×10^{-2}	2.55×10^{-2}	1.13×10^{-2}	2.57×10^{-3}	1,78	4,33	4.13×10^{-1}	1.01×10^{-1}	4.80×10^{-3}	8.0×10^{-3}	7.12×10^{-3}	1588,173	2076,143	1953,109

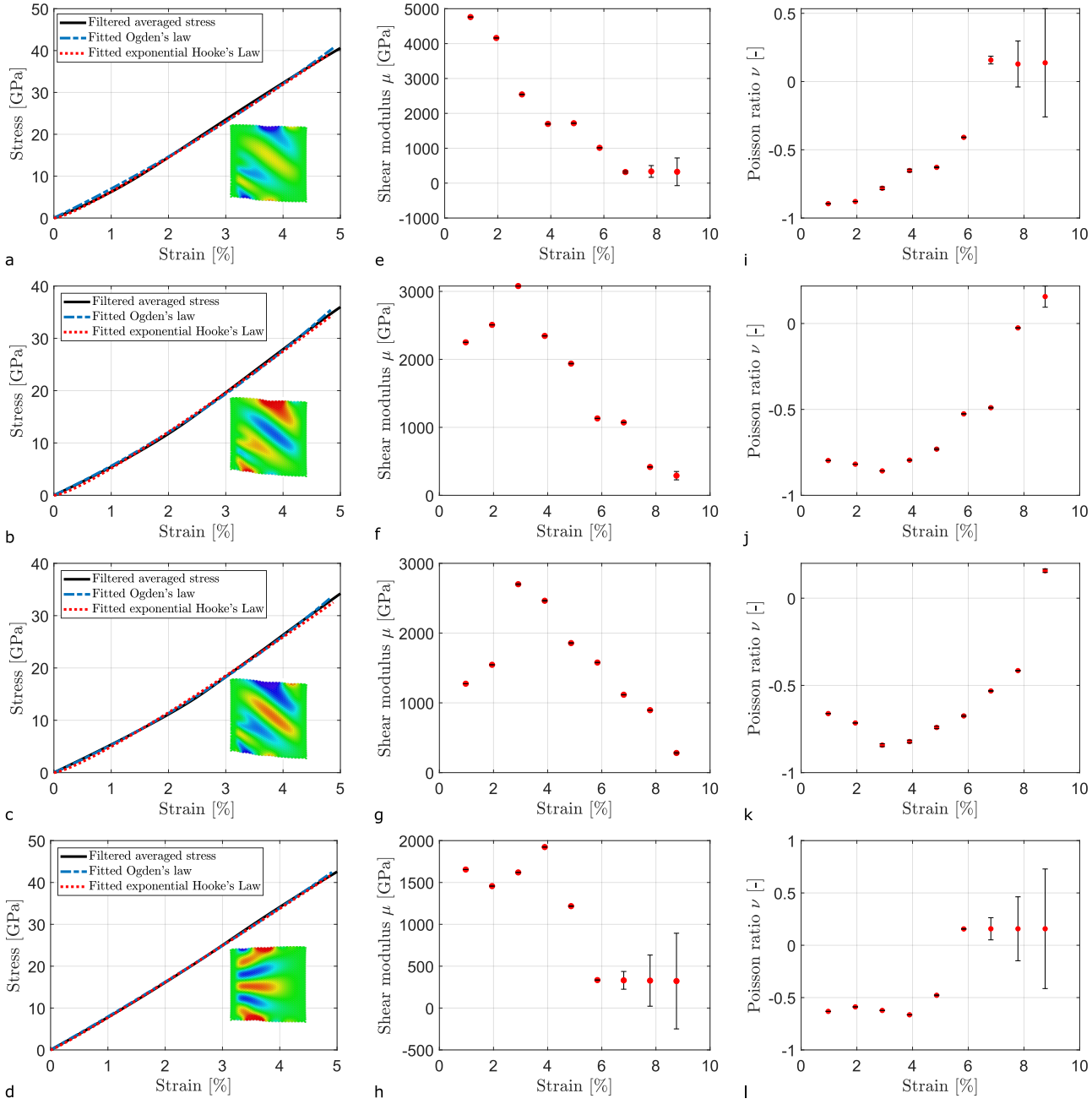

FIG. 8: a-d show the fitting of the exponential Hooke's law and Ogden's law to the filtered average stress data from MD simulations. e-h show the shear modulus of the sample obtained from fitting Ogden's law to the filtered average stress data at different strain-rates. i-l show the Poisson's ratio of the sample obtained from fitting Ogden's law to the filtered average stress data at different strain-rates. Vertical lines indicate the proportional squared sum of residuals.

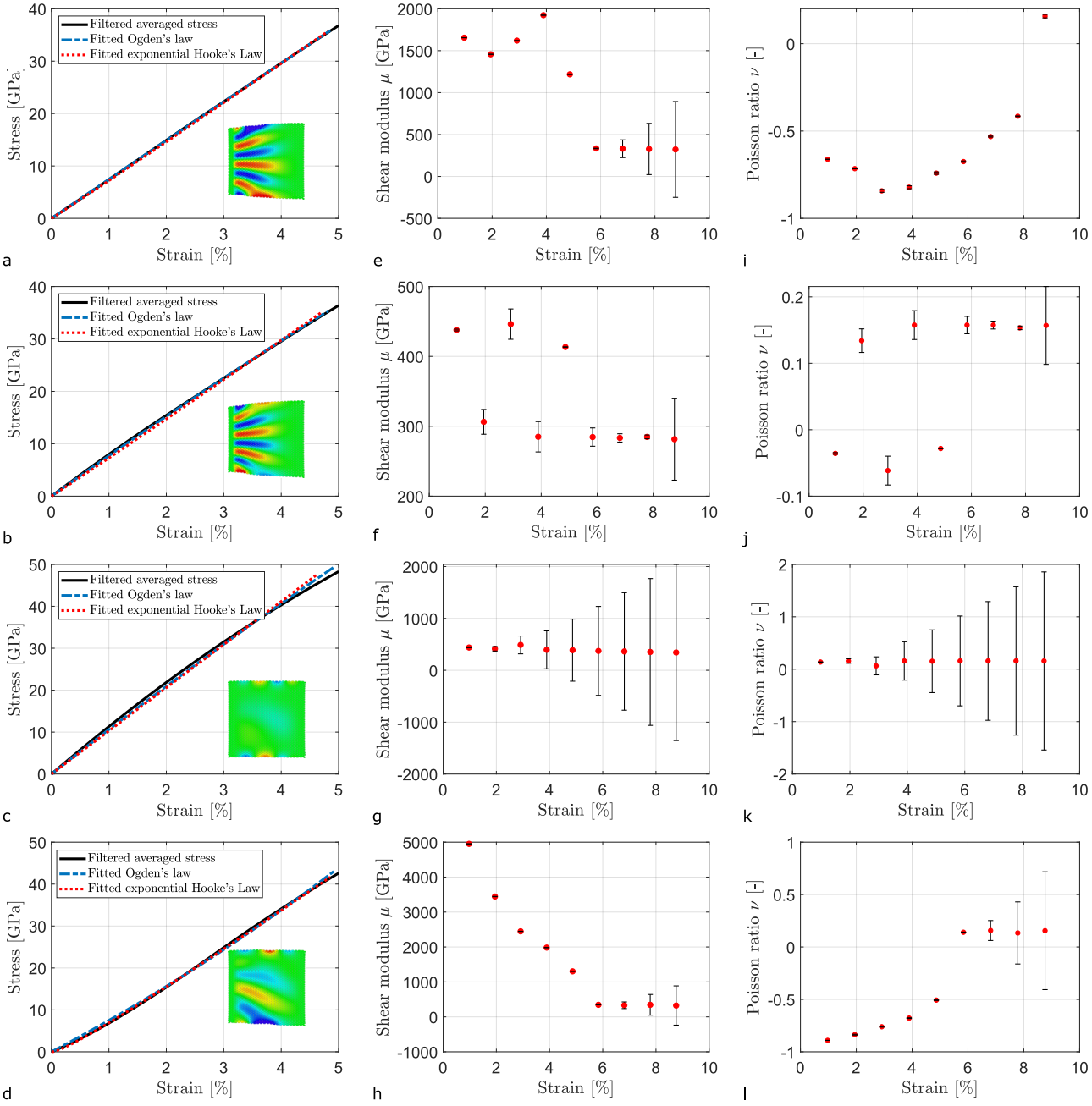

FIG. 9: a-d show the fitting of the exponential Hooke's law and Ogden's law to the filtered average stress data from MD simulations. e-h show the shear modulus of the sample obtained from fitting Ogden's law to the filtered average stress data at different strain-rates. i-l show the Poisson's ratio of the sample obtained from fitting Ogden's law to the filtered average stress data at different strain-rates. Vertical lines indicate the proportional squared sum of residuals.

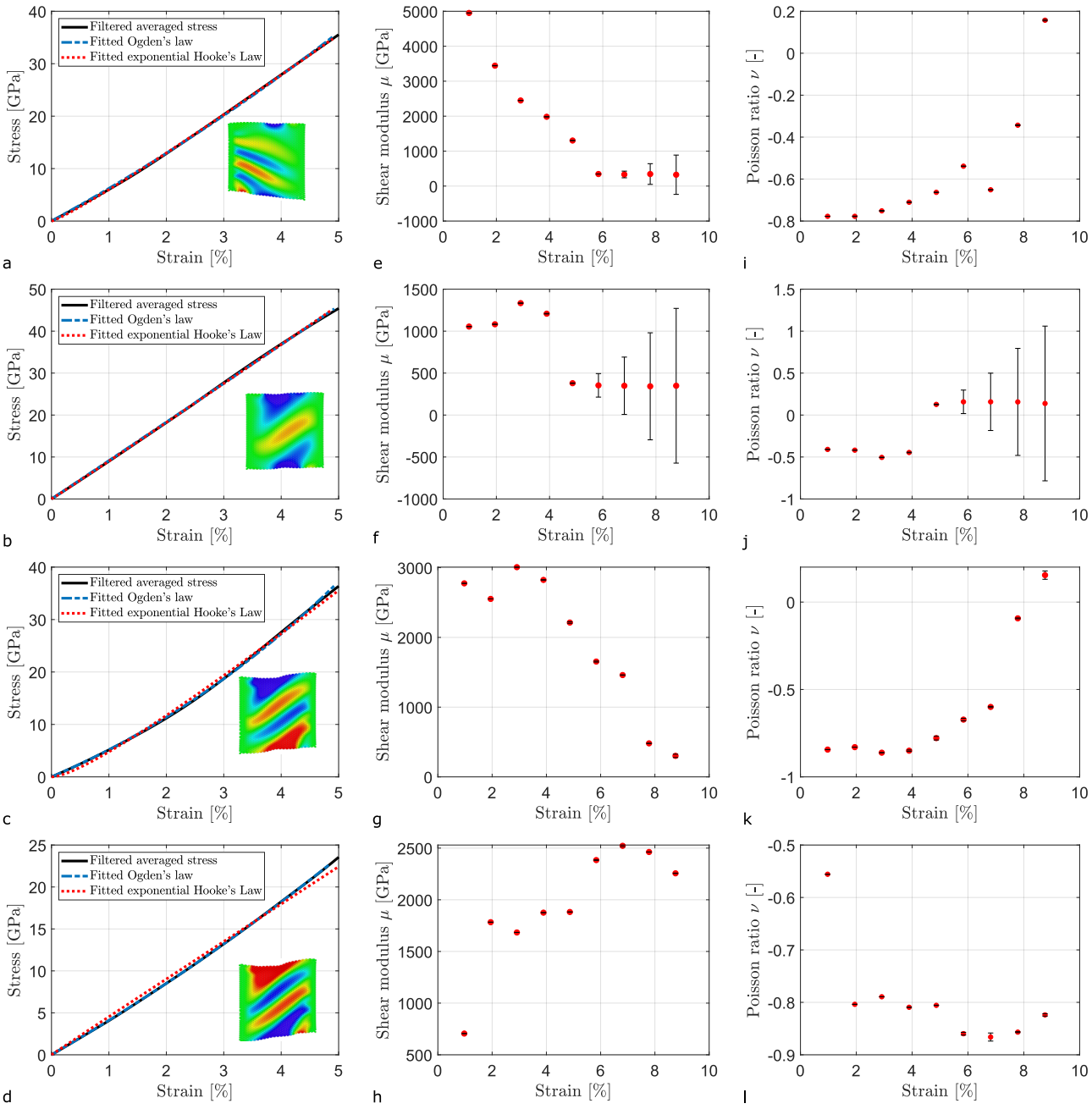

FIG. 10: a-d show the fitting of the exponential Hooke's law and Ogden's law to the filtered average stress data from MD simulations. e-h show the shear modulus of the sample obtained from fitting Ogden's law to the filtered average stress data at different strain-rates. i-l show the Poisson's ratio of the sample obtained from fitting Ogden's law to the filtered average stress data at different strain-rates. Vertical lines indicate the proportional squared sum of residuals.

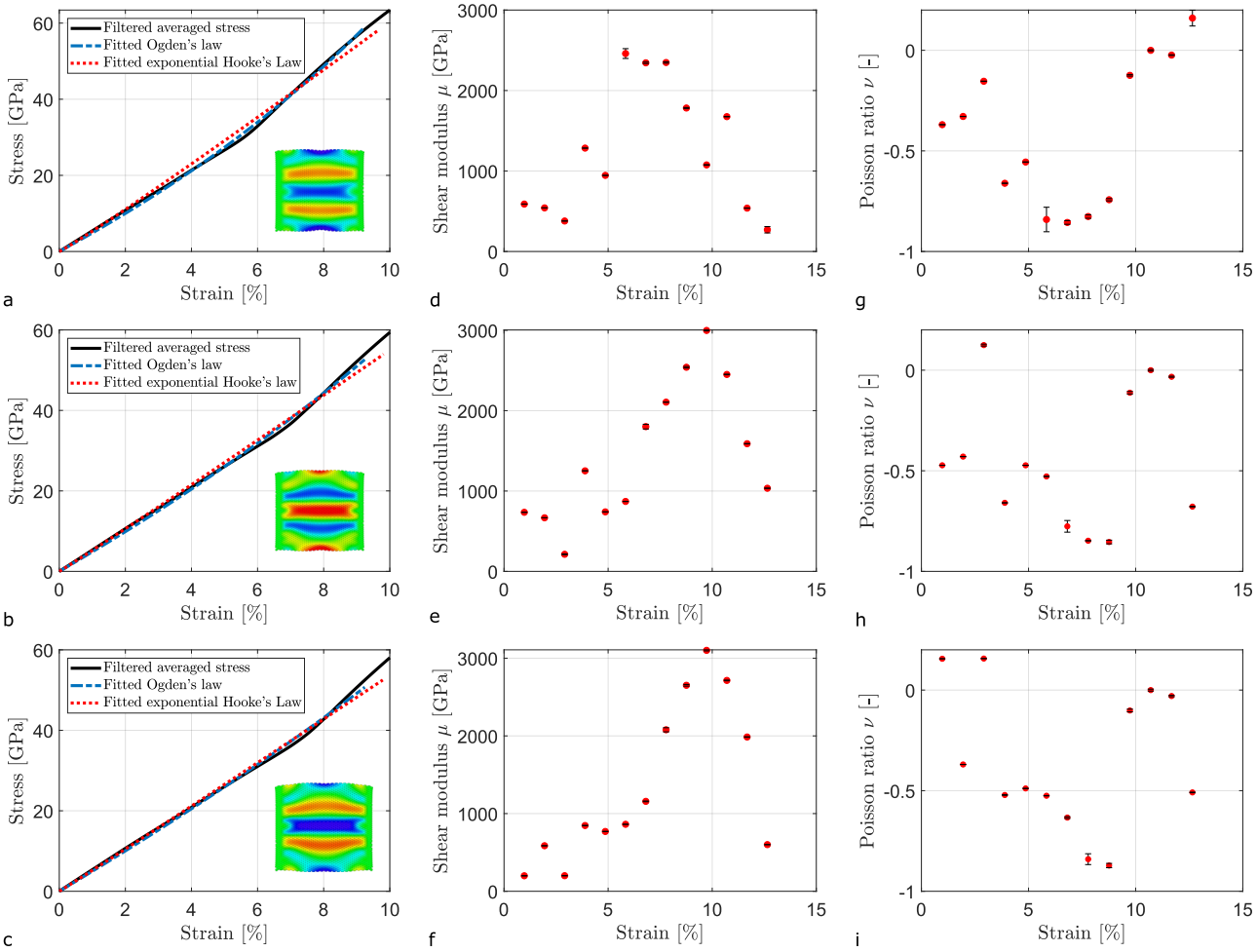

FIG. 11: a-c show the fitting of the exponential Hooke's law and Ogden's law to the filtered average stress data from MD simulations. d-f show the shear modulus of the sample obtained from fitting Ogden's law to the filtered average stress data at different strain-rates. g-i show the Poisson's ratio of the sample obtained from fitting Ogden's law to the filtered average stress data at different strain-rates. Vertical lines indicate the proportional squared sum of residuals.

S4: COMPARISON OF THE EFFECT OF DYNAMIC RIPPLES AND STATIC WRINKLES ON THE MECHANICAL RESPONSE

Earlier research showed that static wrinkling is dominant over dynamic rippling in the nonlinear behaviour [19, 28]. For the wrinkled layers of this research it comes clear that the nonlinearity due to wrinkling has a larger effect than the nonlinearity caused by rippling. This is due to the fact that the wrinkles in our samples have much higher amplitudes than ripples.

To investigate if wrinkles also dominate in simulations were both ripples and wrinkles are present a wrinkled sample was simulated at 300 K. By comparing the stress-strain curves obtained for 1 K and 300 K it was observed that there is almost no difference, as can be seen in figure 12.

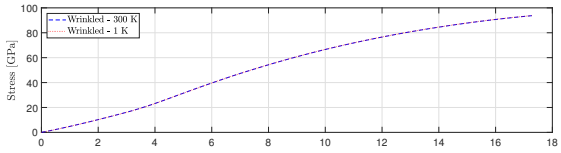

FIG. 12: Stress-strain curve of a wrinkled layer at 1 K and 300 K

* Electronic mail: l.dijkink@student.tudelft.nl
† l.dijkink@student.tudelft.nl

[1] J. N. Grima, S. Winczewski, L. Mizzi, M. C. Grech, R. Cauchi, R. Gatt, D. Attard, K. W. Wojciechowski, and J. Rybicki, Advanced Materials **27**, 1455 (2015).
[2] R. J. Nicholl, N. V. Lavrik, I. Vlassiouk, B. R. Srijanto, and K. I. Bolotin, Physical Review Letters **118** (2017), 10.1103/PhysRevLett.118.266101.
[3] M. D. Stoller, S. Park, Z. Yanwu, J. An, R. S. Ruoff, Y. Zhu, J. An, R. S. Ruoff, Z. Yanwu, J. An, and R. S. Ruoff, Nano Letters **8**, 3498 (2008).
[4] C. Liu, Z. Yu, D. Neff, A. Zhamu, and B. Z. Jang, Nano Letters **10**, 4863 (2010).
[5] H. Wang, K. Sun, F. Tao, D. J. Stacchiola, and Y. H. Hu, Angewandte Chemie - International Edition **52**, 9210 (2013).
[6] A. C. Ferrari, F. Bonaccorso, V. Fal'ko, K. S. Novoselov, S. Roche, P. Bøggild, S. Borini, F. H. Koppens, V. Palermo, N. Pugno, J. A. Garrido, R. Sordan, A. Bianco, L. Ballerini, M. Prato, E. Lidorikis, J. Kivioja, C. Marinelli, T. Ryhänen, A. Morpurgo, J. N. Coleman, V. Nicolosi, L. Colombo, A. Fert, M. Garcia-Hernandez, A. Bachtold, G. F. Schneider, F. Guinea, C. Dekker, M. Barbone, Z. Sun, C. Galiotis, A. N. Grigorenko, G. Konstantatos, A. Kis, M. Katsnelson, L. Vandersypen, A. Loiseau, V. Morandi, D. Neumaier, E. Treossi, V. Pellegrini, M. Polini, A. Tredicucci, G. M. Williams, B. Hee Hong, J. H. Ahn, J. Min Kim, H. Zirath, B. J. Van Wees, H. Van Der Zant, L. Occhipinti, A. Di Matteo, I. A. Kinloch, T. Seyller, E. Quesnel, X. Feng, K. Teo, N. Rupesinghe, P. Hakonen, S. R. Neil, Q. Tannock, T. Löfwander, and J. Kinaret, Nanoscale (2015), 10.1039/c4nr01600a.
[7] M. Gikunda and P. Thibado, Bulletin of the American Physical Society (2018).
[8] K. N. Kudin, G. E. Scuseria, and B. I. Yakobson, Physical Review B **64**, 235406 (2001).
[9] F. Liu, P. Ming, and J. Li, Physical Review B - Condensed Matter and Materials Physics **76**, 1 (2007).
[10] R. Ansari, S. Ajori, and B. Motevalli, Superlattices and Microstructures **51**, 274 (2012).
[11] Y. Fu, T. Ragab, and C. Basaran, Computational Materials Science **124**, 142 (2016).
[12] M. C. Wang, C. Yan, L. Ma, N. Hu, and M. W. Chen, Computational Materials Science **54**, 236 (2012).
[13] B. Mortazavi and S. Ahzi, Carbon **63**, 460 (2013).
[14] A. Tapia, R. Peón-Escalante, C. Villanueva, and F. Avilés, Computational Materials Science **55**, 255 (2012).
[15] B. Sajadi, F. Alijani, D. Davidovikj, J. H. Goosen, and P. G. Steeneken, **234302** (2017).
[16] H. TERRONES and A. MACKAY, The Fullerenes **30**, 113 (1993).
[17] H. Qin, Y. Sun, J. Z. Liu, M. Li, and Y. Liu, Nanoscale **9**, 4135 (2017).
[18] W. Gao and R. Huang, Journal of the Mechanics and Physics of Solids **66**, 42 (2014).
[19] S. Lee, Nanoscale Research Letters **10** (2015), 10.1186/s11671-015-1135-5.
[20] R. J. Nicholl, H. J. Conley, N. V. Lavrik, I. Vlassiouk, Y. S. Puzyrev, V. P. Sreenivas, S. T. Pantelides, and K. I. Bolotin, Nature Communications **6**, 1 (2015).
[21] B. Rakshit and P. Mahadevan, Physical Review B - Condensed Matter and Materials Physics **82**, 1 (2010).
[22] B. Sajadi, S. van Hemert, B. Arash, P. Belardinelli, P. G. Steeneken, and F. Alijani, Carbon **139**, 334 (2018).
[23] A. Fasolino, J. H. Los, and M. I. Katsnelson, Nature Materials **6**, 858 (2007).
[24] B. Sajadi, S. Wahls, S. v. Hemert, P. Belardinelli, P. G. Steeneken, and F. Alijani, Journal of the Mechanics and Physics of Solids **122**, 161 (2019).
[25] C. Lee, X. Wei, J. W. Kysar, and J. Hone, Science **321**, 385 (2008).
[26] E. Cadelano, P. L. Palla, S. Giordano, and L. Colombo, Physical Review Letters **102**, 1 (2009).
[27] Y. Wei, B. Wang, J. Wu, R. Yang, and M. L. Dunn, Nano Letters **13**, 26 (2013).

[28] I. V. Gornyi, V. Yu Kachorovskii, and A. D. Mirlin, 2D Materials **4** (2017), 10.1088/2053-1583/4/1/011003.
[29] S. Plimpton, "Fast parallel algorithms for short-range molecular dynamics," (1995).
[30] K. Zhao, K. Min, and N. Aluru, Nano Letters , 1 (2009).
[31] J. Tersoff, Physical Review Letters **61**, 2879 (1988).
[32] F. Gayk, J. Ehrens, T. Heitmann, P. Vorndamme, A. Mrugalla, and J. Schnack, *Young's moduli of carbon materials investigated by various classical molecular dynamics schemes*, Tech. Rep.
[33] S. J. Stuart, A. B. Tutein, and J. A. Harrison, Citation: J. Chem. Phys **112**, 6472 (2000).
[34] D. Brenner, Physical Review B **42**, 9458 (1990).
[35] V. M. Pereira, A. H. Castro Neto, H. Y. Liang, and L. Mahadevan, Physical Review Letters **105**, 1 (2010).
[36] A. Stukowski, K. Albe, O. Actis, M. Brodski, M. Erdmann, and a. , Modelling Simul. Mater. Sci. Eng **18**, 15012 (2010).
[37] M. Amabili, *Nonlinear Mechanics of Shells and Plates in Composite, Soft and Biological Materials* (Cambridge University Press, 2018).
[38] R. W. Ogden, *Large deformation isotropic elasticity-on the correlation of theory and experiment for incompressible rubberlike solids*, Tech. Rep. (1972).
[39] R. Hill, Advances in Applied Mechanics **18**, 1 (1979).
[40] B. Storakers, *J. Me& Phys. Solids*, Tech. Rep. 2 (1986).
[41] X. Liu, T. H. Metcalf, J. T. Robinson, B. H. Houston, and F. Scarpa, Nano Lett **12**, 1 (2012).
[42] K. Min and N. R. Aluru, Applied Physics Letters **98**, 1 (2011).
[43] K. V. Zakharchenko, M. I. Katsnelson, and A. Fasolino, Physical Review Letters **102**, 2 (2009).

5

Paper: Is a single layer graphene cantilever stable?

Is a single layer graphene cantilever stable?

Laura Dijkink, Farbod Alijani, Peter G. Steeneken, Banafsheh Sajadi

Abstract

Graphene has extracted tremendous attention to use in nanoelectromechanical devices. Single layer graphene cantilevers show great potential, however due to the difficult manufacturing of these fragile structures they remain virtually unstudied. Herein, we investigate, by simple experiments with a cantilever sheet made of paper and molecular dynamics simulations of graphene cantilevers, the possibilities of stabilising graphene cantilevers by implying a curvature. We find that, depending on the aspect ratio and ratio of curvature, single layer graphene cantilevers can be stabilised by implying a curvature.

Keywords: Graphene, Cantilever, Graphene, Molecular Dynamics, Stability, Curvature

1. Introduction

Due to the extraordinary mechanical and electrical properties of graphene it has received substantial interest for applications in the nanoelectromechanical (NEMS) applications, such as mass sensors and high frequency resonators. Though many breakthroughs in graphene research have resulted in a better understanding of the mechanical properties of graphene, more research is needed to reach the full potential of applications. Two important configurations, among others, to investigate the mechanical properties of graphene are singly and doubly clamped beams. Doubly clamped beams have been extensively studied in the last years. At the same time graphene cantilevers remain virtually unstudied, mainly due to the difficult construction of these delicate structures. Despite this limited research it was already stated that graphene cantilevers have potentially more applications due to the linear behaviour and high sensitivity [1].

Researchers applied different approaches to tune the stability, or in other words, tune the bending rigidity of graphene cantilevers. Increasing the number of layers is one of the approaches used by researchers [2, 3]. Recently researchers demonstrated a method to fabricate single layer graphene cantilevers (SLGCs) by stabilising them with multiwalled carbon nanotube elements [4]. All these methods add extra material to the system. Recent research suggested that the stiffness of thin sheets in general can be largely increased by implying a transversal curvature [5]. Since graphene layers are inherently wrinkled in the out-of-plane direction [6], resulting in a curved surface, it is interesting to investigate if those wrinkles could stabilise SLGCs.

In this work the effect of different rates of two-dimensional bending on the stiffness of thin sheets with different aspect ratios is investigated. To this end simple experiments using paper sheets as well as molecular dynamics simulations of single layer graphene cantilevers are performed.

2. Method

The effect of curvature on the stability of thin sheets was investigated on cantilevers with the same aspect ratios both on the macroscopic- and the nanoscale. At the macroscopic scale simple experiments were performed using a cantilever sheet made of paper to investigate the general principle. Paper sheets have been used before to demonstrate the effect of transversal curvature on the bending stiffness of thin sheets [5]. In this work, three cantilevers were investigated with three different aspect ratio: 1:5, 1:2.5 and 1:1.25. The investigated sheets have sizes of 300 mm by 60 mm (sheet 1), 150 mm by 60 mm (sheet 2) and 75 mm by 60 mm (sheet 3). One short end of the sheet was fixed to a static table to create a cantilever. Two-dimensional bending was implied by moving the top and bottom boundaries of the fixed end 7.5 mm towards each other, demonstrated in figure 1.

Figure 1: Visualisation of implying a transversal curvature by moving the boundaries towards each other. Dotted line indicates the flat configuration. Solid line indicates curved configuration.

Molecular dynamics simulations on graphene sheets were performed using large-scale atomic/molecular massively parallel simulator software (LAMMPS) [7]. Pristine single layers of graphene with aspect ratio's of again 1:5, 1:2.5 and 1:1.25 were investigated, using graphene sheets with dimensions of 100 Å by 500 Å, 100 Å by 250 Å and 100 Å by 125 Å. These sizes are large enough to ignore the size effect of graphene [8]. Simulations were performed with a timestep of 1 fs, periodic boundary conditions were applied and the Tersoff potential is used. Simulations were executed at 1 K, therefore the layers were first thermalized in the NVT ensemble. During thermalization one short boundary was fixed in the x-, y- and z-direction, the other

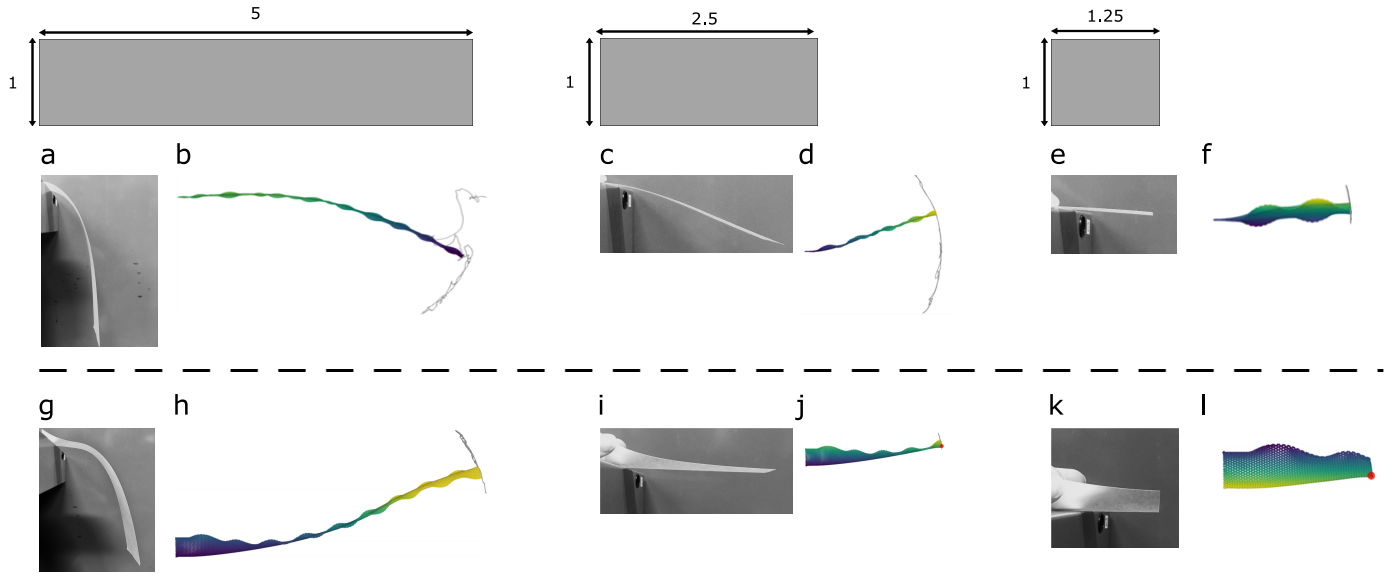

Figure 2: Stability of thin cantilevers. a-f) Snapshots of the investigated cantilevers, without two-dimensional bending, a,c,e are paper sheets; b,d,f are graphene sheets. g-l) Snapshots of the investigated cantilevers, with two-dimensional bending, g,i,k are paper sheets; h,j,l are graphene sheets.

short boundary was fixed in the z-direction and the long boundaries were free to move, to make sure that no internal stresses were build up during thermalization. To create a curved surface the long top and bottom boundaries were moved towards each other with a velocity of 0.1 Å ps^{-1} in the NPT ensemble for certain amounts of time to create different rates of curvature. The rate of curvature is expressed as the amount of displacement of both boundaries towards the middle. Next the system was relaxed for 0.5 ns with the short boundaries fixed in all directions. Finally the cantilever structure was formed by releasing one of the short boundaries. The system was then relaxed for 5 ns, after which the free vibration continued for another 5 ns.

3. Results and discussion

Instability of cantilevers is in our work defined as deflection of the end point of the cantilever. Figure 2a-f show snapshots of the investigated cantilevers, without two-dimensional bending. Figure 2a shows the paper sheet with an aspect ratio of 1:5. This sheet largely bends downwards due to the gravitational force working on the paper. Figure 2c and 2e show the paper sheets with aspect ratio of 1:2.5 and 1:1.25, respectively. Comparing the three paper sheets with each other it is noted that, as expected from theory, the deflection of the end-point becomes smaller when the aspect ratio decreases.

Figure 2b, 2d and 2f show the single layer graphene sheets with the same aspect ratio's. Although no curvature is implied, it is noted that all sheets have 'warped' edges. Warping of the edges inherently occurs in single layer graphene cantilevers because of edge-stresses [9]. Looking at the deflection of the graphene sheets, indicated by the grey-lines, it can be seen that all cantilevers deflect. The deflections were found in a range of 270 Å for the biggest layer to 30 Å for the smallest layer. In accordance with what was found for the paper sheets, the layer becomes more stable, in terms of end-displacements, if the aspect ratio becomes smaller. Movement of free-standing graphene cantilevers is caused by thermal fluctuations, instead of driven by gravitational forces working on the cantilevers. According to theory, the predicted root mean square amplitude of thermal fluctuation driven fluctuations is given by:

$$x_{th}^2 = 2\sqrt{\frac{k_B T L^3}{Y h^3 b}}, \tag{1}$$

where k_B, T, L, Y, h, and b are the Boltzmann constant, the temperature of the environment, the length, the Young's modulus, thickness, and width of the graphene cantilever. To predict the amplitudes an effective thickness of 0.13 nm is used instead of the physical thickness of one carbon atom [4]. According to this formulation the oscillations of the cantilevers should vary between 0.7 Å and 5.6 Å. It is noticed that the oscillation amplitudes predicted by equation 1 are not agreeing with the values from molecular dynamics.

As have been mentioned before, two-dimensional bending could greatly increase the stiffness of thin membranes against bending. Figure 2g-l show snapshots of the investigated cantilevers, with two-dimensional bending. It must be noted that the rate of curvature of both the paper sheets and the graphene sheets are the same. Figure 2g shows the curved paper sheet with an aspect ratio of 1:5, compared to figure 2a it can be seen that the total deflection of the end-point is much smaller. Also, it can be seen that the sheet does not bend downwards close to the curved boundary, which means that part of the cantilever is stable. The smaller layers, shown in figure 2i and figure 2k, do not bend at all, so they are completely stable due to the transversal curvature. This experiment shows that two-dimensional bending can increase the bending stiffness of thin sheets resulting in (partially) stable cantilevers, depending on the aspect ratio.

Figure 2h, figure 2j and figure 2l show the curved graphene cantilevers modelled in MD. The deflections of the end-points

are 95 Å for sheet 1, 40 Å for sheet 2 and less than 1 Å for sheet 3. Comparing these amplitudes with the previously obtained amplitudes of the flat configurations it can be observed that the amplitudes of the curved configurations are much smaller for all sheets. By taking a closer look at the movement it can be seen that sheet 3 is fully stabilised due to the implied curvature, whereas sheet 1 and 2 are only stable close to the fixed left boundary. It is noted that the phenomenon seen in the simple paper sheet experiments holds for single layer graphene sheets as well.

Our experiments indicated that the stability is depending on the aspect ratio of the cantilever. To investigate the effect of different rates of curvature, expressed as the amount of displacement of both boundaries towards the middle, on the stability different rates of curvature were implied to the largest graphene sheet (figure 2h). In figure 3 the motion of the cantilever ends of this sheet can be seen for different rates of curvature. It can be seen that the stable area, defined as the area with less than 1 Å out-of-plane displacement and depicted by the red line, will become larger for larger rates of curvature. On the other side, the out-of-plane motion of the cantilever end is not becoming smaller for larger rates of curvature. This experiment therefore suggests that the stable area could increase due to an increase in the rate of curvature.

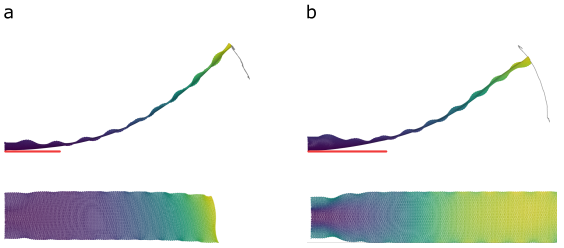

Figure 3: Images of trajectories (grey lines) of sheet 1 with different rates of curvature. a) 2.5 Å b)10 Å. The red line illustrates the stable area.

4. Conclusion

In conclusion, we presented that transversal curvature of thin cantilevers reinforces the mechanical stability of these structures. Depending on the aspect ratio and rate of curvature the stability is local or global. We were able to simulate curved single layer graphene cantilevers using atomistic modelling techniques. Carrying out these simulations in real experiments is a rich avenue for future investigation. In the end, with these simulations we provide new insight for designing and investigating the next generation of graphene nanoelectromechanical devices.

[1] P. Li, Z. You, T. Cui, Graphene cantilever beams for nano switches, Applied Physics Letters 101 (9) (2012) 093111. doi:10.1063/1.4738891.
URL http://aip.scitation.org/doi/10.1063/1.4738891

[2] A. Reserbat-Plantey, L. Marty, O. Arcizet, N. Bendiab, V. Bouchiat, A local optical probe for measuring motion and stress in a nanoelectromechanical system, Nature Nanotechnology 7 (3) (2012) 151–155. doi:10.1038/nnano.2011.250.

[3] Y. Yuasa, A. Yoshinaka, T. Arie, S. Akita, Visualization of vibrating cantilevered multilayer graphene mechanical oscillator, Applied Physics Express 4 (11). doi:10.1143/APEX.4.115103.

[4] O. V. Martynov, M. Bockrath, Carbon nanotube stabilized single layer graphene cantilevers, Applied Physics Letters 110 (15). doi:10.1063/1.4979837.

[5] V. Pini, J. J. Ruz, P. M. Kosaka, O. Malvar, M. Calleja, J. Tamayo, How two-dimensional bending can extraordinarily stiffen thin sheets, Scientific Reports 6 (2016) 1–16. doi:10.1038/srep29627.

[6] R. J. Nicholl, H. J. Conley, N. V. Lavrik, I. Vlassiouk, Y. S. Puzyrev, V. P. Sreenivas, S. T. Pantelides, K. I. Bolotin, The effect of intrinsic crumpling on the mechanics of free-standing graphene, Nature Communications 6 (2015) 1–7. doi:10.1038/ncomms9789.
URL http://dx.doi.org/10.1038/ncomms9789

[7] S. Plimpton, Fast parallel algorithms for short-range molecular dynamics (1995). doi:10.1006/jcph.1995.1039.

[8] K. Zhao, K. Min, N. Aluru, Chirality and Size Dependent Elastic Properties of Silicene Nanoribbons under Uniaxial Tension, Nano Letters (Md) (2009) 1–6. doi:10.1021/nl901448z.
URL http://www.gruppofrattura.it/ocs/index.php/ICF/icf13/paper/do

[9] V. B. Shenoy, C. D. Reddy, A. Ramasubramaniam, Y. W. Zhang, Edge-stress-induced warping of graphene sheets and nanoribbons, Physical Review Letters 101 (24) (2008) 2–5. doi:10.1103/PhysRevLett.101.245501.

III

Closing

6

Conclusions and Recommendations

The objective of this work was to contribute to the understanding of the mechanical response of single layered graphene beams, singly and doubly clamped, with surface imperfections. For the doubly clamped beam the goal was to find a constitutive model capable of describing the behaviour during the transition from the wrinkled state to the flat state. The objective for singly clamped beams was to stabilise them by making use of two-dimensional bending. To this end both molecular dynamics and continuum modelling methods have been employed. This section reports the main conclusions of these methods. Additionally, recommendations for further research are discussed.

6.1. Conclusions

Wrinkled graphene in molecular dynamics The molecular dynamics models developed could be used to investigate the effects of surface corrugations on both singly and doubly clamped beams adequately. The model developed of a doubly clamped beam can be used to investigate the formation of wrinkles and the transition from the wrinkled state to the flat state in great detail. Besides this, single layer graphene as well as multilayer graphene beams could be investigated within the developed framework. In addition, multiple wrinkling patterns could be established due to the parametrized boundary condition. By adding or changing the values of the parameters of the parametrized boundary condition a different wrinkle pattern will occur. In this research equibiaxial stretching is applied, but uniaxial stretching could be used as well within the framework. The model developed of a single layer cantilever shows the motion of different sizes of cantilevers as well as the motion of cantilevers with different rates of curvature.

Wrinkled graphene in continuum mechanics A continuum model in the FEM software COMSOL is developed to investigate the formation of wrinkles in graphene nanoribbons. Formation of endless possibilities of wrinkle patterns could be investigated in the provided framework, due to the use of a parametrized boundary condition. The obtained model cannot be used to investigate the transition from the wrinkled state to the flat state as a result of the high sensitivity of the model.

Constitutive models Different models have been investigated to describe the nonlinear stress-strain relation during the transition from the wrinkled state to the flat state of graphene nanoribbons. Although literature suggests that the presented exponential Hooke's law describes the transition from the wrinkled state to the flat accurately, from this research it is concluded that the exponential Hooke's law fails to do so. The transition point between the nonlinear behaviour during flattening and the linear behaviour after flattening is underestimated. Also, the predicted values of fitting parameter α are five to ten times higher than the values mentioned in literature. The transition from the wrinkled state to the flat state is however very accurately described by the first order compressible Ogden's law. Furthermore Ogden's law provides insights into the shear modulus and Poisson's ratio during stretching. Ogden's law predicts a decreasing shear modulus and an increasing Poisson's ratio after flattening. Also, Ogden's law predicts a negative Poisson's ratio for wrinkled graphene membranes at small strains.

Stability of a single layer graphene cantilever We present that transversal curvature of single layer graphene cantilevers reinforce the mechanical stability of the structures. Depending on the aspect ratio and rate of curvature the stability is local or global.

Wrinkling in presence of ripples It is concluded that for our samples wrinkling is dominant over rippling.

Contribution to science The novelty of this work lies mainly in the exploration of different constitutive models to describe the mechanical behaviour of wrinkled graphene membranes during the transition from the wrinkled state to the flat state. Also, this exploration provides more insights into the mechanical properties of wrinkled graphene membranes. It shows the possibilities of tailoring the mechanical properties of graphene by making use of surface corrugations, instead of focusing on removing them. Next, a lot of research has already investigated defect induced wrinkles and the formation of one type of wrinkles or ripples in graphene layers, however, investigation of the formation and effects of different wrinkling patterns in pristine graphene is not a framework I came across in literature. With this research we provide new insights for designing and investigating the next generation of graphene nanoelectromechanical devices.

6.2. Recommendations

To complement the contents of this thesis, experiments of both single layer wrinkled nanocantilevers as well as wrinkled nanoribbons could be carried out to establish whether the proposed conclusions hold in real life as well.

For the investigation of nanoribbons specific the following recommendations are suggested. Our results suggest that a higher wrinkling amplitude result in earlier rupture of the layer if equibiaxial stretching is applied, it would be interesting to investigate this phenomenon in more detail. The continuum model could be improved to a model capable of describing the transition from the wrinkled state to the flat state. In this research 15 samples of nanoribbons were established in molecular dynamics and evaluated in detail afterwards. It would be interesting to investigate more samples, in MD or CM, with different wrinkle height and patterns. Furthermore, if a lot more samples were investigated, the machine learning framework presented could be extended to develop an algorithm capable of predicting the parameters of a constitutive model based on a set of micro-structure descriptors.

For the research into the stabilisation of single layer graphene cantilevers the following recommendation is proposed. Investigating the effect of a curved surface consisting of consecutive formations of folds on the stability would be interesting.

In general, tailoring the mechanical properties of graphene in an experimental setting is an interesting field for future research.

IV

Appendix - Rectangular Ribbon

A

Continuum mechanics model

This appendix presents the methodology applied to develop a continuum mechanics model of a wrinkled rectangular ribbon of graphene. Also, results of preliminary analyses are presented and discussed. Calculations were performed in the COMSOL Multiphysics®software.

A.1. Description of the Finite Element Model

To investigate the mechanical behaviour of wrinkled rectangular ribbons of graphene during the transition from the wrinkled state to the flat state a continuum model is developed. The simulation is decomposed into the following tasks: (1) initial conditions, (2) linear buckling analysis to obtain the different mode shapes, (3) establish wrinkled configuration and (4) equibiaxially stretching of wrinkled configuration to flatten the wrinkled membrane. The different tasks are explained in more detail in the following subsections.

A.1.1. Initial conditions

At the start of the simulation the initial state of the system has to be provided. The first step is to define the geometry, a 100 Å by 100 Å flat layer was formed in the xy-plane. Since the thickness of the layer is much smaller than the length and the width of the layer, shell elements are used. Finally the flat layer of graphene is meshed using a fine triangular mesh.

A.1.2. Linear buckling analysis

To transform the flat layer to a wrinkled layer a shear is applied at one of the boundaries. To get insight in how much shear is needed to wrinkle the layer a linear buckling analysis is performed. In this analysis the right boundary is fixed in all directions, while a parametrized shear is applied at the left boundary:

$$v = 0.1\left(c_1 \sin\left(\frac{\pi y}{100}\right) + c_2 \sin\left(\frac{2\pi y}{100}\right) + c_3 \sin\left(\frac{3\pi y}{100}\right) + c_4 \sin\left(\frac{4\pi y}{100}\right) + c_5 \sin\left(\frac{5\pi y}{100}\right) + c_6 \sin\left(\frac{6\pi y}{100}\right)\right), \tag{A.1}$$

where $c_1 - c_6$ are between -3 and $+3$. To include deformations geometric nonlinearities are included in all steps of the model. The critical loads and corresponding mode shapes from the linear buckling analysis are used as initial conditions in the next step of the simulation.

A.1.3. Create wrinkled structure from buckling analysis

The next step is to really convert the flat layer to a wrinkled layer. The solutions from the previous step are used as initial values of the variables solved for in this step. Next, shear is applied in small steps, 1 Å per step, up to the critical load obtained in the linear buckling analysis at the left boundary. The right boundary is fixed in all directions. By applying a different parametrized boundary condition different wrinkled configurations can be created.

A.1.4. Stretch layer

After the wrinkled layers are generated the layers must be stretched equibiaxially to obtain the stress-strain curves. Again, the solutions from the previous step are used as initial values of the variables solved for in this step. The final shear of the previous step is applied at the left boundary to maintain the wrinkled structure at the start. Next, the layer is equibiaxially stretched in small steps of 0.01 Å up to 7 Å in all directions.

A.2. Results of preliminary analyses

Preliminary analyses were carried out to address several simulation issues related to modelling of graphene membranes, in particular the formation of the wrinkles in the graphene membrane.

A.2.1. Wrinkling hierarchy

In the final model it was decided to create wrinkles by applying a shear at the left boundary, however, it is also possible to create wrinkles by stretching the layer or compressing the layer [14, 57]. Wrinkles will appear in a membrane when the displacement applied results in a stress higher than the stress needed to have wrinkles. Different approaches have been tested to come to the best approach for our research. In this preliminary analysis a constant displacement is applied instead of the parametrized displacement mentioned in the previous section.

Wrinkling under tension To create wrinkles under tension a displacement is applied at the left boundary of the layer in the x-direction. The resulting modeshapes can be seen seen in figure A.1. It can be seen that the critical displacement is much higher than 20 % strain, which is the strain at which graphene will break. Therefore it was concluded that creating wrinkles by applying tension is not possible.

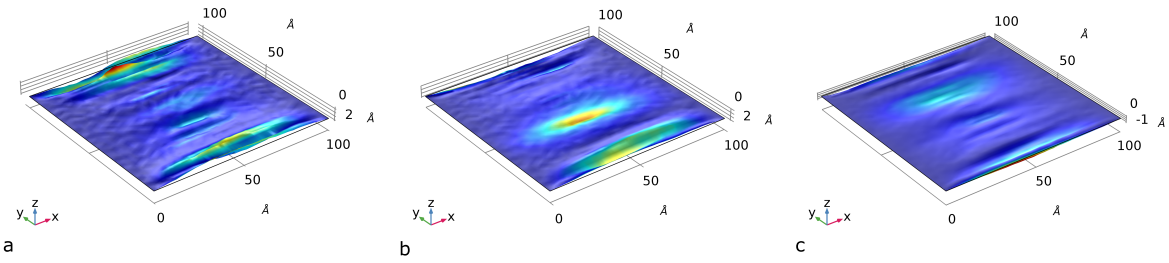

Figure A.1: Different modeshapes of a thin layer under increasing compression, critical displacements are: a) 2.94×10^5 Å, b) 5.89×10^5 Å, c) 8.66×10^5 Å. Colours indicate out-of-plane displacement.

Wrinkling under compression In this approach wrinkles are created by applying a compressive displacement at the left boundary of the layer. The resulting modeshapes can be seen in figure A.2. It can be seen that wrinkles are induced unidirectional and perpendicular to the displacement direction.

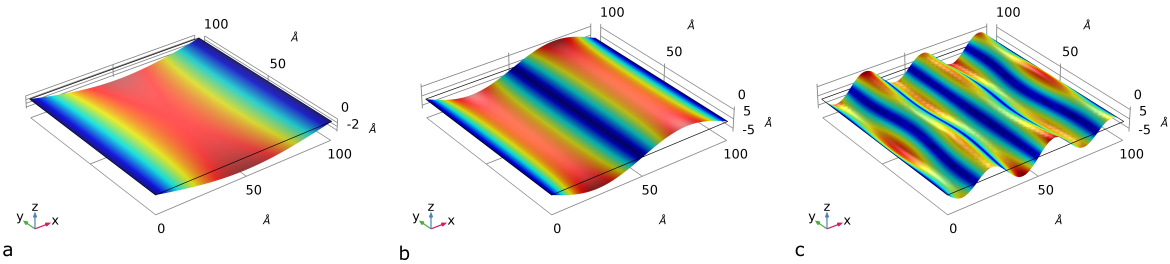

Figure A.2: Different modeshapes of a thin layer under increasing compression, critical displacements are: a) 0.0934 Å, b) 0.376 53 Å, c) 3.0652 Å. Colours indicate out-of-plane displacement.

Wrinkling under shear In this approach wrinkles are created by applying a shear displacement at the left boundary of the layer. The resulting modeshapes can be seen in figure A.3. Wrinkles are formed under an angle of 45°.

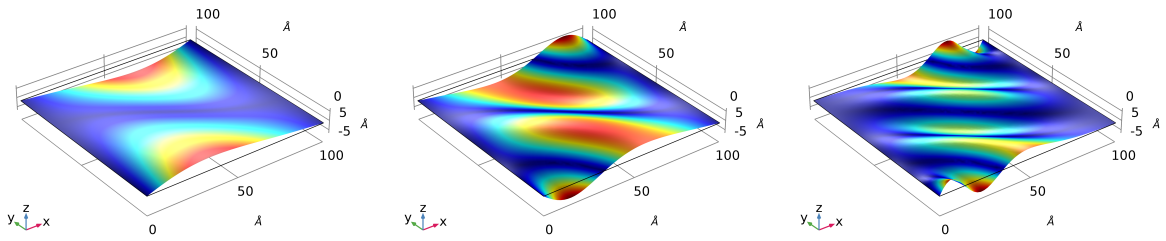

Figure A.3: Different modeshapes of a thin layer under increasing shear, critical loads are: a) 0.974 66 Å, b) 2.4577 Å, c) 6.9644 Å

From this preliminary analysis it was concluded that wrinkles could be induced by compressing the membrane, or by applying a shear at the boundaries. Both methods will be tested in molecular dynamics.

A.2.2. Establishing the wrinkled membrane

After the linear buckling analysis the modeshapes obtained should be used in the next step of the model. Different approaches have been tested to establish the wrinkled layer. One approach of creating the wrinkled configuration is by re-meshing the shapes obtained from the linear buckling analysis, however, this is not possible if shell elements are used. Another easy way of creating a wrinkled surface is by applying a surface displacement. However, this surface displacement is a fixed configuration, since we want to investigate the transition from the wrinkled state to the flat state, we cannot use this approach. It is also possible to give the system an initial surface displacement. However, since the boundaries will stay in the old position, this initial surface displacement will disappear. From the previous approaches it was concluded that the correct boundary conditions must be applied to make sure that the wrinkled configuration given will stay at the start. However, by only applying a shear strain the layer did not transform to the wrinkled state. Therefore, it was concluded that the correct boundary conditions must be applied as well as the initial surface displacement.

A.2.3. Results after stretching

If the wrinkled configuration is established the transition from the wrinkled state to flat state can be investigated. Unfortunately it turned out that the model was to sensitive, therefore the result were different for different processors. Thus, the stress-strain curves obtained were not used in this research.

B

Molecular dynamics model of rectangular ribbon of graphene

Molecular dynamics (MD) simulations were performed using the large-scale atomic/molecular massively parallel simulator (LAMMPS) software [56]. This appendix presents the methodology applied to develop a molecular dynamics model to investigate the formation of wrinkles in a graphene membrane as well as the transition from the wrinkled state to the flat state of a rectangular ribbon of graphene. Also, results of preliminary analyses are presented and discussed. Preliminary analyses were carried out to address several simulation issues related to modelling of graphene membranes.

B.1. Important concepts in molecular dynamics

Molecular dynamics is the term used to describe simulations consisting of the step-by-step numerical solution of the classical equations of motion. First the forces acting on the atoms must be found, these are usually derived from the integration of a potential function. Next, the equations of motion are integrated. Different types of algorithms can be used to perform this integration. In the end, MD simulations produce dynamical trajectories for a system composed of N particles.

Define microstate using statistical-mechanical ensembles LAMMPS makes use of ensembles to define the state of the system. Different algorithms are used to maintain a certain state. Different ensembles exist with different characteristics, an overview is given in table B.1. For different parts of the simulation different ensembles were chosen.

Table B.1: Different ensembles and there characteristics

NVE	Microcanonical Ensemble	fixed number of atoms, N; fixed volume, V; fixed energy, E
NVT	Canonical Ensemble	fixed number of atoms, N; fixed volume, V; fixed temperature, T
NPT	Isobaric-Isothermal Ensemble	fixed number of atoms, N; fixed pressure, P; fixed temperature, T

Calculate forces using potential functions Molecular dynamics uses either quantum mechanics, Newton's law of motion, empirical data or a mixed model to define a potential function. The accuracy of the result of the simulation depends on the correct choice of potential function. In chapter 2, a few of the many interatomic potentials that have been developed and used in graphene research are mentioned. It has been shown that the AIREBO and Tersoff potential can accurately compute the bond-bond interaction, bond breaking, and bond reforming in the carbon atoms. Also, the AIREBO potential takes the long-range Lennard-Jones potential into account. If graphene consisting of multiple layers is investigated a potential must be used which takes those long-range interactions into account. If we are dealing with a single layer of graphene, the Tersoff potential can be used.

Integration algorithms To solve the potential function numerical algorithms have been developed for integrating the equations of motion. Algorithms accelerate the atoms in the direction of the force. To choose which algorithm to use especially the computational efficiency is important. It is favourable to have a algorithm of low order, to allow for an increased time step as much as possible without threaten the ensemble. A commonly used algorithm is the Verlet algorithm, which is a compact and accurate algorithm. Another often used algorithm is the reversible reference system propagator algorithm (RESPA), which is known for greatly reducing the CPU time for systems which require small time steps. The Verlet algorithm as well as the RESPA has been tested, it was concluded that the RESPA was not significantly faster than Verlet algorithm, therefore the Verlet algorithm was chosen.

B.2. Description of the Molecular Dynamics model of a single layer ribbon

In the following paragraphs the different steps of the model to investigate both the formation of wrinkles in and the transition from the wrinkled state to the flat state of a ribbon of graphene are explained. This section is based on the documentation of LAMMPS.

B.2.1. Initial conditions

At the start of the simulation the initial state of the system has to be provided. This means that the type of atoms, units, cut-off length, boundary conditions, potential function and size of time steps must be defined.

In all simulations unit style 'metal' is used, which means that the mass is given in $\mathrm{g\,mol^{-1}}$, distances are given in Å, time in ps, energy in eV, temperature in K and pressure in bar. Periodic boundary conditions for the simulation box were applied. Tersoff potential is chosen, since previous research showed that the Tersoff potential can accurately compute the bond-bond interaction, bond breaking, and bond reforming in the carbon atoms [34]. An extra cut-off length of 2.0 Å is given. By making the cut-off distance longer more atoms will be in the neighbor list. The advantage of this is that if two atoms move towards each other after moving away from each other, the bond is still listed, which will in the end speed up the computation. For numerical stability and accuracy a correct time step must be chosen, typically one that is at least on order of magnitude smaller than the fastest time scale in the system. If the time step is to large, the system will become unstable. A time step of 1 fs is used in all simulations.

B.2.2. Construct layer

After the initial conditions are provided, a pristine single layer graphene sheet of size 100 Å by 100 Å was constructed in the *xy*-plane. First a hexagonal lattice was created, next graphene atoms were added to the lattice. The result is a pristine layer of graphene, as can be seen in figure B.1. Different selections of atoms are defined, which are the different boundaries needed in the next parts of the simulation.

B.2.3. Relaxation

To make sure that the system has no potential problems during computation the potential energy has to be minimised, in other words, the system must be relaxed. Relaxation means minimising the potential energy, before computing other things. This part is performed in the NVT ensemble. Different relaxation algorithms can be used, in this case the Polak-Ribiere algorithm is used. Stopping criteria are 1×10^{-10} eV for the potential energy and 1×10^{-10} $\mathrm{eV\AA^{-1}}$ for the force. To prevent curling of the membrane all out-of-plane coordinates are fixed.

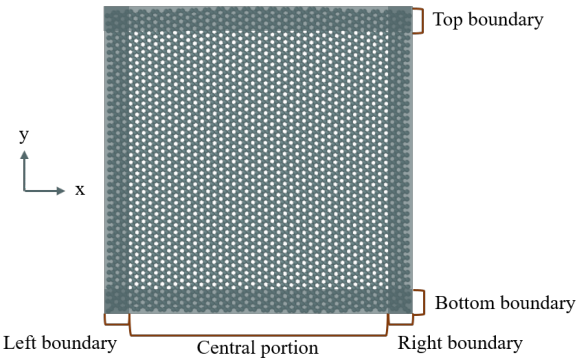

Figure B.1: The layer being modelled and the boundary conditions used. The columns of atoms on the side are used to hold the system in-plane and to apply the mechanical loads.

B.2.4. Thermalization

The minimised system can be seen as a structure being at 0 K. To run a simulation at a certain temperature the system must be heated up to this certain temperature, this is done during thermalisation. During thermalisation energy flows in the system by means of accelerating each atom. After a certain time the system is converged to the Maxwell-Boltzmann distribution. Also, during thermalisation part of the potential energy will be moved to kinetic energy, thus graphene will develop Brownian motion. It is important to thermalise the system for a long time to make sure it is converged.

Our system is thermalized for 20 ps, which is long enough to reach the converged state at 1 K. At this low temperature almost no Brownian motion will be developed. Thermalization is performed in the NVT ensemble, to make sure that the number of atoms, volume and temperature are constant. To prevent tensioning of the membrane, caused by the negative thermal expansion of graphene, the layer is free to move in the x - and y-direction, but the left and right boundary are fixed in the out-of-plane direction.

B.2.5. Create wrinkles

Wrinkles in the graphene layer are created by moving the boundaries. Different commands can be used in LAMMPS to move atoms:

- Fix deform erate — Changes box dimension at a constant engineering strain rate.
- Displace atoms — Displaces the group of atoms by the specified third displacement vector.
- Surface displacement — Move the atoms in z-direction directly
- Fix move — Performs updates of position and velocity for atoms in the group each timestep.

Preliminary analyses showed that only the *fix move* command resulted in a stable wrinkled layer. Thus, the wrinkled structure is created by moving the left boundary using the *fix move* command. The velocity is parametrized using the following formula, to create different configurations:

$$v = 0.1\left[c_1 \sin\left(\frac{\pi y}{100}\right) + c_2 \sin\left(\frac{2\pi y}{100}\right) + c_3 \sin\left(\frac{3\pi y}{100}\right) + c_4 \sin\left(\frac{4\pi y}{100}\right) + c_5 \sin\left(\frac{5\pi y}{100}\right) + c_6 \sin\left(\frac{6\pi y}{100}\right)\right], \tag{B.1}$$

where $c_1 - c_6$ are between -3 and $+3$. This part of the simulation is performed in the NPT ensemble at zero pressure. The shear is applied for 0.05 ns after which the system is relaxed for 0.5 ns.

B.2.6. Stretch and relaxation

After the wrinkled layers are formed the layer must be stretched equibiaxially to obtain the stress-strain curves. Again this done by moving the boundaries using the *fix move* command. The atoms in the boundaries were bounded in the z direction, to obtain a more realistic situation, as if it was gripped to horizontal rollers. Furthermore, this constraint makes sure that the sheet stays parallel to the xy-plane.

The layer is stretched equibiaxially at a constant strain-rate of 0.0005 Å/fs at all sides. The strain is applied for 0.5 ns after which the system is relaxed for the same amount of time. This strain-increment was applied 40 times, so the layer is stretched 10 Å in all directions, which corresponds with 20 % strain.

B.3. Crumpled and rippled ribbon

To compare the effects of wrinkles with dynamic rippling and crumpling, rippled and crumpled layers are constructed as well. Since most steps are comparable to the steps of the wrinkled-layer-model, these models will not be discussed in detail.

B.3.1. Rippled layer

- Initial conditions — No differences with wrinkled layer
- Construct layer — No differences with wrinkled layer
- Relaxation — No differences with wrinkled layer
- Thermalization — The system is thermalized at 300 K
- Create wrinkles — Not part of this model
- Movement — Extra step in the simulation
- Stretch and relaxation — Other ensemble; lower velocity

To investigate the dynamic corrugations of the system a very small velocity is applied, after which the system is simulated for 0.1 ns. This is long enough to develop vibrations. This simulation is performed in the NVE ensemble only for the atoms not in the boundaries. If the boundary atoms are included the system won't reach convergence and will explode.

The stretching was performed at a velocity 10× lower than the stretching velocity of the wrinkled model, this to prevent bond-breaking. Also, this part of the simulation was performed in the NVE ensemble only for the atoms not in the boundaries.

B.3.2. Crumpled layer

- Initial conditions — No differences with wrinkled layer
- Construct layer — No differences with wrinkled layer
- Relaxation — No differences with wrinkled layer
- Thermalization — The system is thermalized at 300 K
- Create wrinkles — NPT ensemble only applied to atoms not in the boundaries
- Stretch and relaxation — NVT ensemble only applied to atoms not in the boundaries

Wrinkle creation and stretching ensembles are both applied to atoms not in the boundary section. If the boundary atoms were included the system won't reach convergence and will explode.

B.4. Results of preliminary analyses

B.4.1. Wrinkling hierarchy

From the continuum mechanics model it was concluded that a wrinkled configuration could be obtained by either compression or a shear strain at the boundaries. Both methods have been tested in molecular dynamics as well.

Wrinkling under compression In this approach wrinkles are created by applying a compressive displacement at the left boundary of the layer. The graphene layer used for this analysis is of size 75 Å by 425 Å. As expected from the continuum mechanics model, the wrinkles are induced uni-directional and perpendicular to the displacement direction. However, the wrinkles are not static, by looking at figure B.2 it can be seen that during relaxation of the system the wrinkles will move through the layer, they continue moving after relaxation.

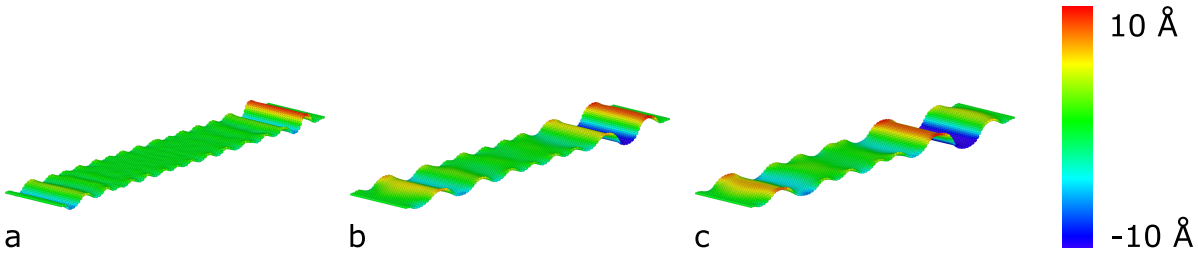

Figure B.2: Wrinkles in graphene layer after moving the left and right boundary 5 Å. Figures are at different timesteps after relaxation: a) 1 ps, b) 3 ps, c)5 ps

Wrinkling under shear In this approach wrinkles are created by applying a shear displacement of 2 Å at the right boundary of the layer. The graphene layer used for this analysis is of size 100 Å by 100 Å for the single layer and 30 Å by 100 Å for the bi-layer. The resulting wrinkled configurations, presented in figure B.3, are both stable.

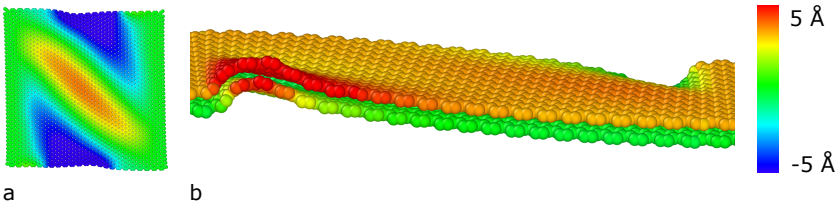

Figure B.3: a) Wrinkling of a graphene layer under shear of 2 Å. b) Wrinkled configuration of a bilayer graphene under shear of 10 Å

C

Machine learning

During the project the idea came up to develop a model able to predict the nonlinearity of the constitutive equations by making use of machine learning techniques. The framework to develop such as model consists of several steps, as can be seen in figure C.1. The framework presented in this appendix is based on the work of M.A. Bessa [10, 11].

The first step is to create the input variables for the machine learning algorithm. This consists of a set of corrugation descriptors and a set of fitting parameters. Next a computational analysis is executed to create the response database. The next step is to apply machine learning to this database to obtain the predictive model. Finally this predictive model could be validated by comparing the results with results from molecular dynamics simulations. The proposed method can be used as an algorithm for characterisation of the mechanical properties of a wrinkled graphene membrane based on the set of corrugation descriptors.

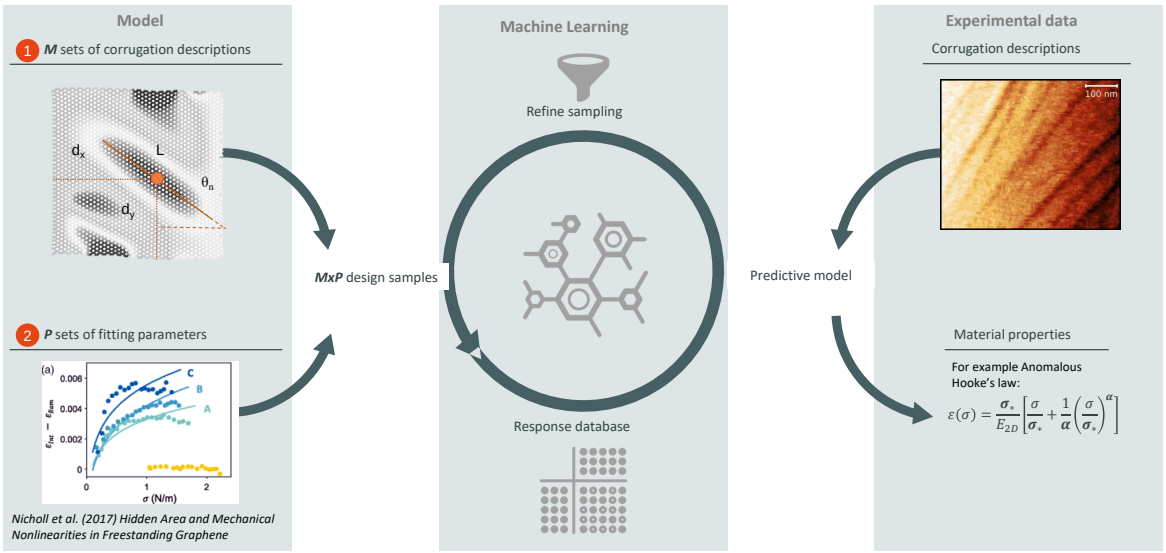

Figure C.1: Schematic of framework of machine learning

Although this framework is not carried out in total, the first parts of the framework have been developed. In the first paper, comments on the hidden area of nonlinearity in graphene, presented in chapter 4, the methodology to come up with a set of fitting parameters was already explained. This appendix will present the methodology to obtain the corrugation descriptors.

C.1. Corrugation descriptors

To investigate the relationship between the wrinkled configurations and the nonlinearity parameters obtained by fitting a constitutive law, a finite set of descriptors to characterise the corrugations must be obtained. In this section the different corrugation descriptors are explained, also the method to obtain these descriptors will be explained in more detail.

C.1.1. Methods

Describing a structure can be done using different approaches, there are two main categories of methods for quantifying the morphology of a system: correlation functions and physical descriptors. Correlation functions describe how variables, such as density, at different positions are related. An often used method is the two-point correlation function, which is accurate as well as computational efficient. This two-point correlation function can be interpreted as the probability that two points at certain positions are both in a certain phase. In our case, the probability that two points will be both in a wrinkled region.

The physical descriptor-based approach on the other hand uses physically meaning full descriptors, like average height of the system, to represent the micro-structure. Different strengths can be identified of the descriptor-based methodology: the characteristics have well-defined physical meaning; the descriptors have high correlation with the material properties; computation cost are low for characterisation of the descriptors. Therefore, this research used a descriptor-based methodology to characterise the wrinkled layers.

C.1.2. Set of descriptors

To represent the morphology of the wrinkled layers three levels of descriptors are used: composition, dispersion and geometry [78]. Composition is the highest level which only captures the homogenised response of the total system, for example different phases in the system. Dispersion descriptors include properties induced by local features, for example the nearest neighbour distance. Geometry descriptors captures the properties of the individual shapes, in our case the individual wrinkle height for example.

In this research a methodology is presented to obtain the key set of descriptors, sufficient to represent the wrinkled configuration but still small enough to be controllable. The first step is to create a large set of descriptors. Next the redundant descriptors must be removed using descriptor-descriptor analysis. Table C.1 shows the non-related descriptors. After the redundant descriptors have been removed, the most signifi-

Descriptor	Definition	Level
z_{avg}	Average height of the layer	Composition
VdivA	Total volume under layer divided by the total area	Composition
n	Total number of wrinkles	Dispersion
H_n	Height of each wrinkle at centerpoint	Geometry
x_n, y_n	Coordinates of the centres of each wrinkle	Geometry
θ_n	Orientation angle of each wrinkle	Geometry
L_n	Length of each wrinkle	Geometry

Table C.1: Set of corrugation descriptors.

cant descriptors should be selected, so the number of features must be reduced while the maximum amount of information is retained. This can be done using unsupervised or supervised learning, where supervised learning uses predetermined classifications. For each descriptor the influence on the parameters from the constitutive fitting is evaluated. From this analysis a certain amount of descriptors can be selected with high impact. The last step is to check the uniqueness of the descriptors, this means checking if multiple wrinkled realisations are possible for one set of descriptors. If this is the case, it should be evaluated if the parameters obtained from the fitting are different as well. If this is the case, the set of descriptor is not unique.

C.1.3. Analysis methodology to obtain descriptors

To extract the descriptors from the output file the Image Processing Toolbox^{TM} in Matlab is used. This section will present the steps taken to extract the descriptors.

1. Load position data at start A 3D-plot is created of the deformed configuration. This 3D-plot is converted to an 2D image.

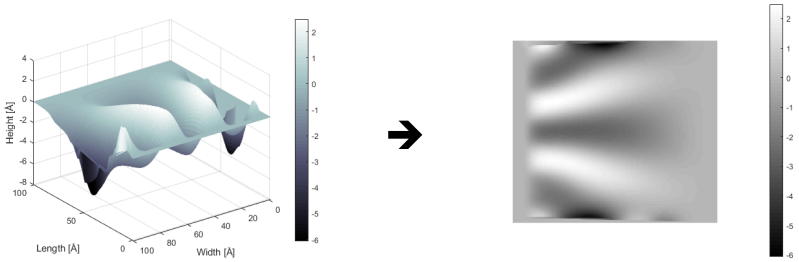

Figure C.2: Left: 3D plot of the wrinkled layer. Right: 2D image of the 3D plot.

2. Detect wrinkled areas The image is turned into a contour-plot with two levels. As can be seen in figure C.3, this contour-plot defines the wrinkled areas. Since the Image Processing Toolbox^{TM} can only investigate white areas this image is converted.

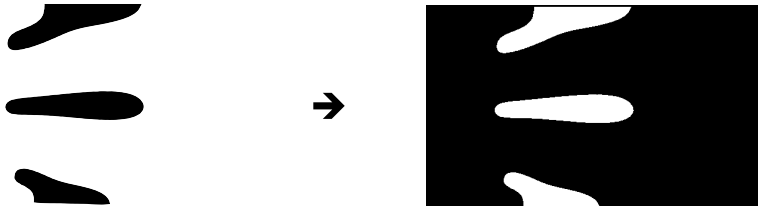

Figure C.3: Left: Contour-plot showing the wrinkled areas in black. Right: Converted images of the contour plot showing the wrinkled areas in white.

3. Extract corrugation descriptors From the contour-plot the descriptors can be extracted using the *regionprops* command of the Image Analysis Toolbox^{TM}. This command measures the properties of the white regions, so the properties of the wrinkled areas. From this analysis the total number of wrinkles, coordinates of the centres of each wrinkle, orientation angle of each wrinkle and the length of each wrinkle are extracted. The average height of the layer and the 'volume divided by the area'-descriptor are calculated from the rough data. The height of each wrinkle at the centerpoint is extracted by finding the intensity of the colour at the specific centers and converting this back into a height.

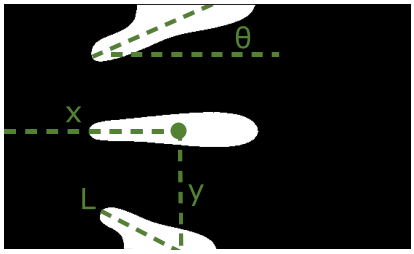

Figure C.4: Schematic of framework of machine learning

D

Extended results

This appendix presents the results which were not presented in the paper 'Comments on the hidden area of nonlinearity in graphene', as presented in chapter 4.

D.1. Out-of-plane displacement during stretching

During the transition from the wrinkled state to the flat state the average out-of-plane displacement of the samples changes. Figures D.2 and D.3 show the average out-of-plane displacements for the different layers during equibiaxially stretching. The out-of-plane displacement decreases up to the transition point, after which bond stretching dominates over dewrinkling. After this transition point either the average out-of-plane displacement stabilises, as can be seen in figure D.2c or increases, as can be seen in figure D.2j for example. This increase is caused by wrinkles at the boundaries. Figure D.1 shows snapshots of sample 11 at different rates of strains. It can be seen that first the wrinkling amplitude decreases, figure D.1a and D.1b, resulting in a decreasing average out-of-plane displacement. Next the wrinkles at the boundaries have an increasing amplitude, figure D.1c and D.1d, resulting in a growing average out-of-plane displacement.

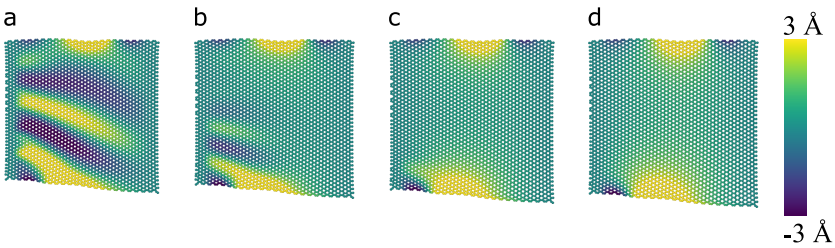

Figure D.1: Snapshots of sample 4.3 at different rates of strain. a) 0 %, b) 3.5 %, c) 7.5 % and d) 9.5 %.

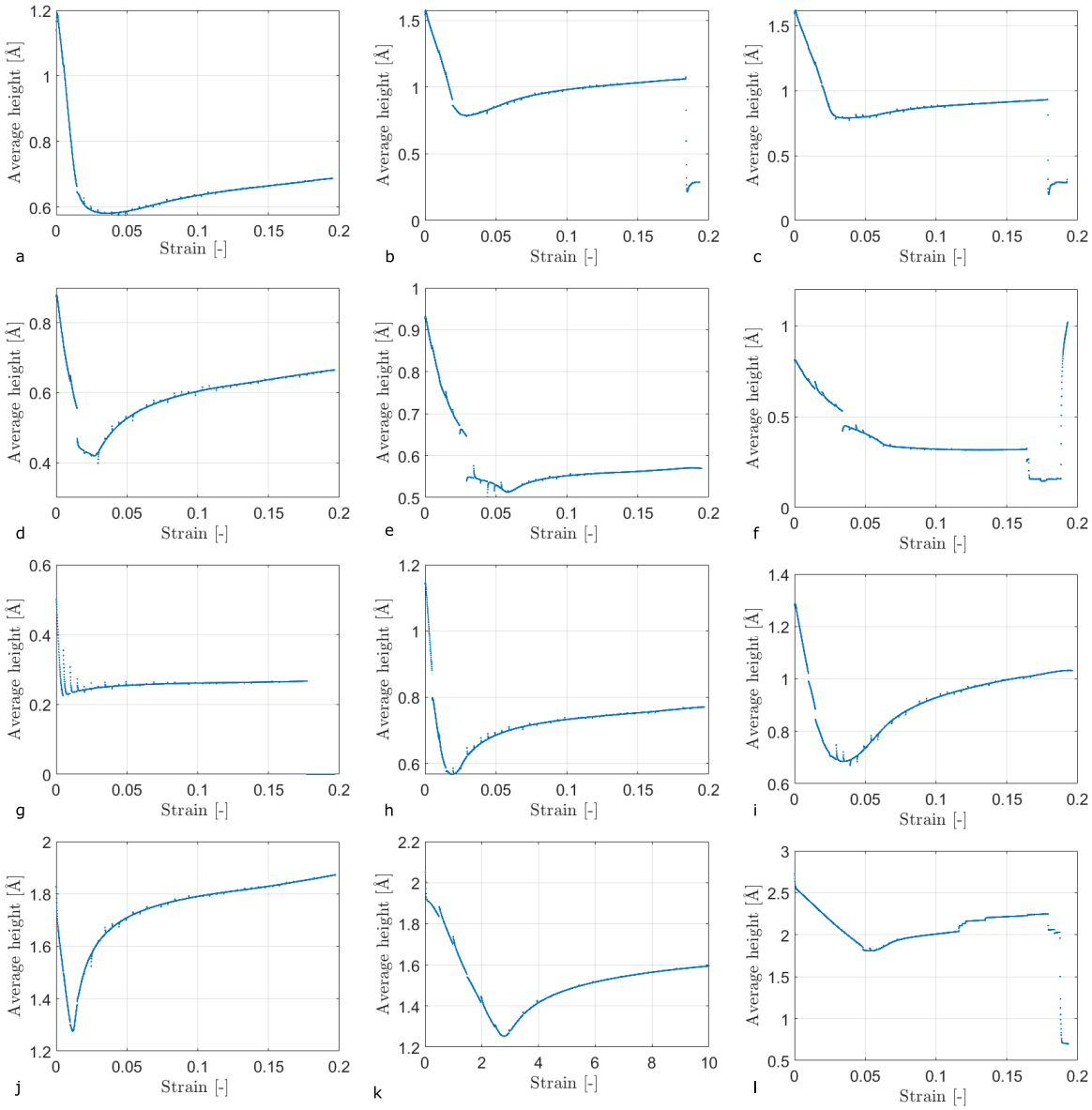

Figure D.2: a-l show the average out-of-plane displacement data obtained with MD simulations for sample 1-12.

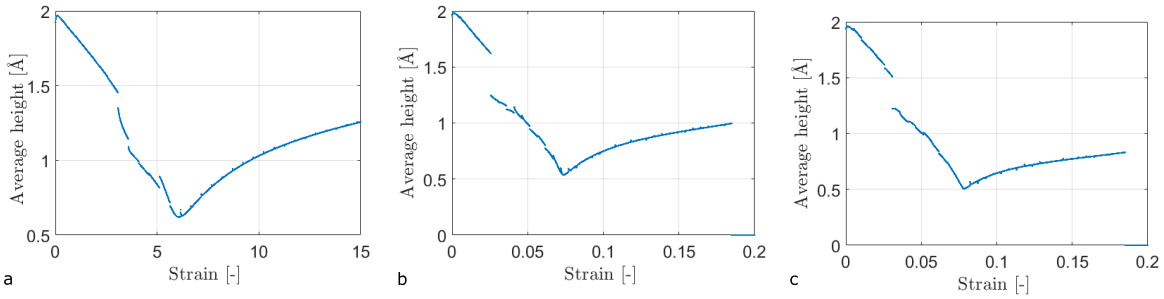

Figure D.3: a-c show the average out-of-plane displacement data obtained with MD simulations for sample 13-15.

D.2. Mechanical response of wrinkled graphene under equibiaxial tension

For the fifteen different samples of this research the mechanical response during equibiaxially stretching is obtained. Figure D.5 and D.6 show all the stress-strain curves obtained for the different configurations. The figures show the filtered stresses in x- and y direction, the raw averaged stress data and the filtered averaged stress data.

The three previously mentioned parts, part I soft nonlinear part, part II linear part, part III yield and fail, could be observed in almost all curves. For samples with very low wrinkling amplitudes the soft nonlinear part is very small (figure D.5g), whereas for samples with high amplitudes rupture starts earlier (figure D.5f).

Although the samples are stretched equibiaxially the stresses in the x- and y-direction are not exactly the same for all samples. This can be explained by the fact that wrinkles are dominant in certain orientations, therefore, softening behaviour can be more dominant in x- or y-direction.

Comparing the stress-strain curves with the curves of the out-of-plane displacement (figure D.2 and figure D.3) it can be seen that the turning points of those figures, the points at which the decrease in amplitude stops, correspond with the points in the stress strain curves where the curve turns linear.

By taking a closer look at the data obtained at very small strains it is observed that the data is scattered at the start, as can be seen in figure D.4. This scattering is caused by numerical instability at the start, therefore the first 15 data-points are excluded in this research.

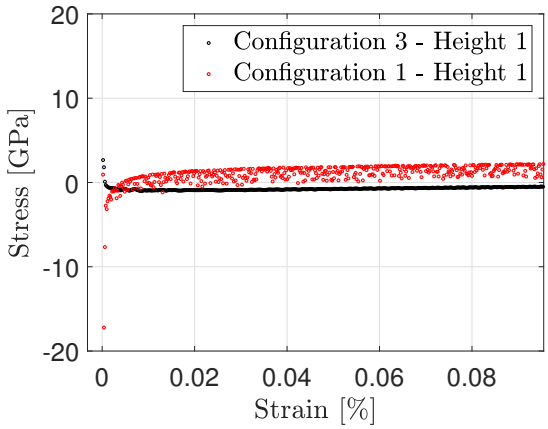

Figure D.4: Nonlinear behaviour at start for two samples. Configuration 1 - height 1 is sample 1. Configuration 3 - height 1 is sample 7.

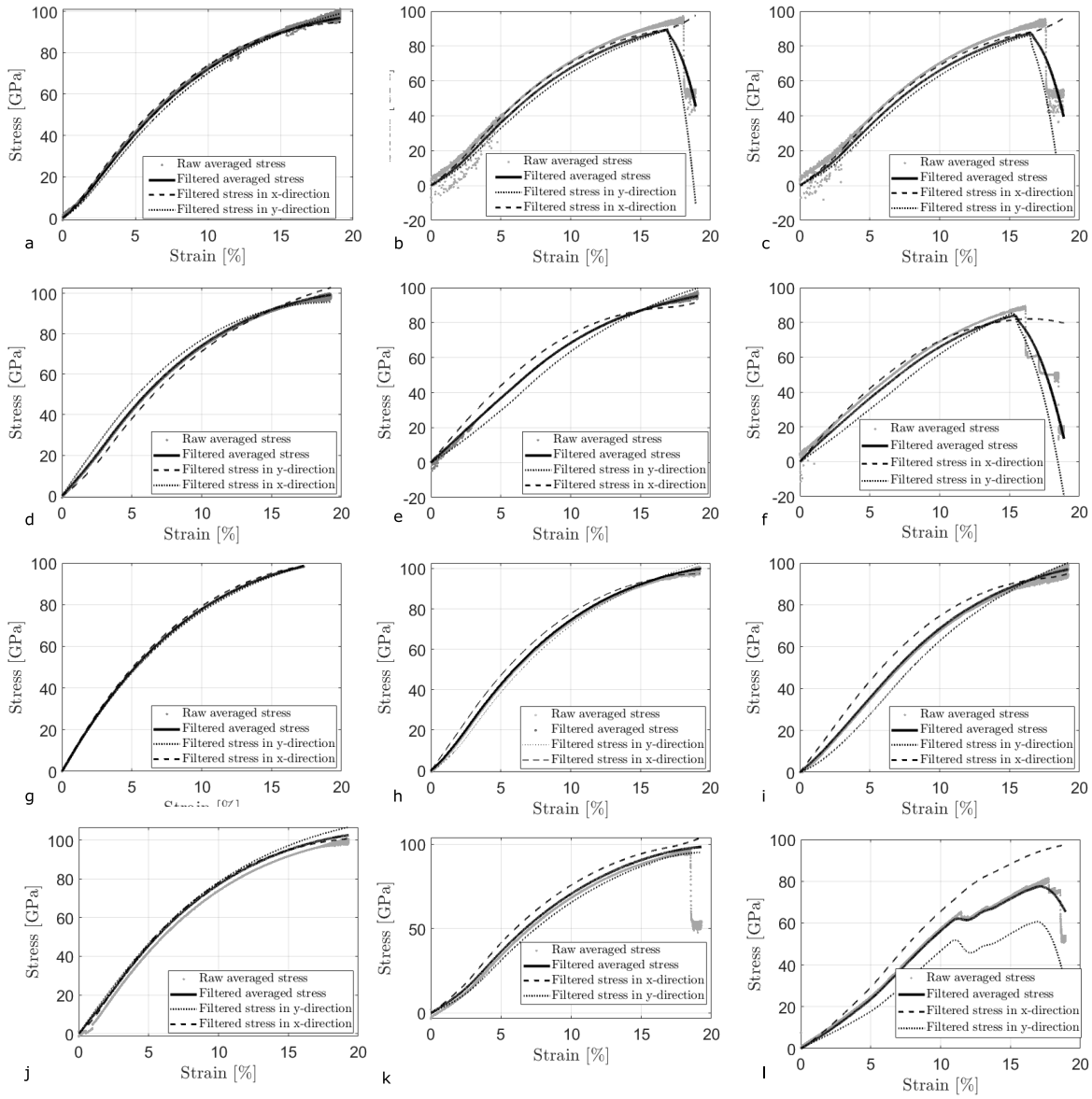

Figure D.5: a-l show the raw and filtered stress strain data of sample 1-12, obtained from MD simulations.

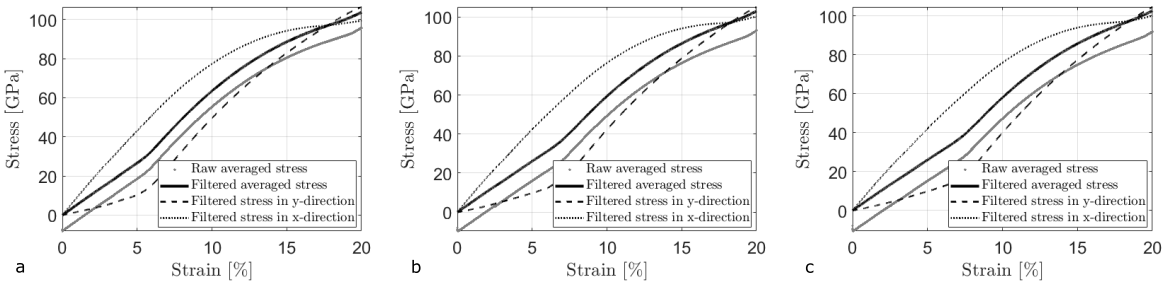

Figure D.6: a-c show the raw and filtered stress strain data of sample 13-15, obtained from MD simulations.

D.3. Crumpled layer

Different researchers stated that static wrinkling is dominant over dynamic rippling [22, 34]. To investigate the interplay between static wrinkling and dynamic rippling a wrinkled layer was simulated at 1 K and 300 K. The resulting corrugation patterns can be seen in figure D.7. The sample at 300 K (figureD.7b) has a slightly higher wrinkling amplitude. Furthermore, ripples can be observed. From figure D.8 it can however be observed that this higher amplitude at the start does not affect the stress-strain curve, since both curves are the same. We propose that this is caused by the fact that amplitudes of ripples are decreasing fast during stretching, compared to the wrinkling amplitude.

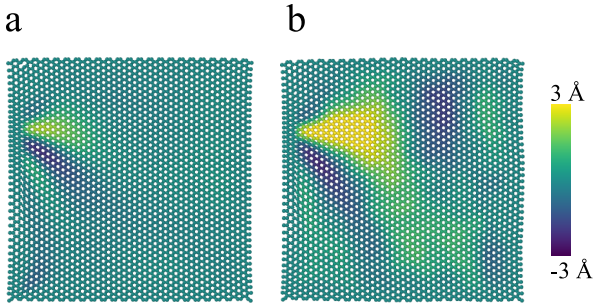

Figure D.7: Snapshots of two samples at 0 % strain with same boundary conditions at different temperatures: a) 1 K, b) 300 K

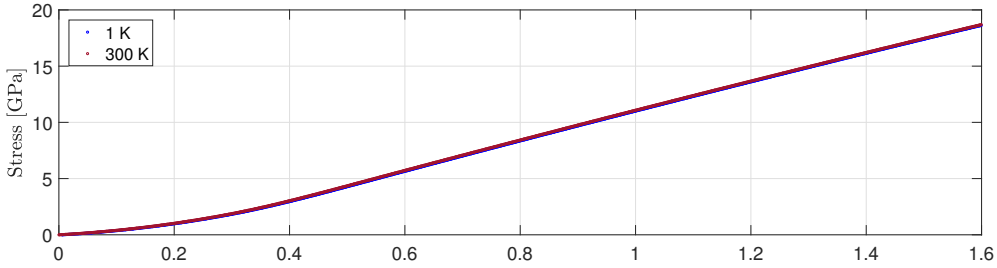

Figure D.8: Stress-strain curve of a wrinkled layer at 1 K and 300 K.

V

Appendix - Cantilever

E

Molecular dynamics model of rectangular cantilever of graphene

This appendix presents the methodology applied to develop a molecular dynamics model to investigate the stability of a wrinkled cantilever of graphene. Results of preliminary analyses are presented and discussed. Important concepts of MD in general have already been discussed in appendix B.

E.1. Description of the molecular dynamics model

In the following paragraphs the different steps to create a model to investigate the stability of a wrinkled cantilever of graphene are explained. This chapter refers to appendix B if similar steps are applied.

E.1.1. Initial conditions

At the start of the simulation the initial state of the system has to be provided. This means that the type of atoms, units, cut-off length, boundary conditions, potential function and size of time steps must be defined. This step is equivalent to the initial conditions step of appendix B.

E.1.2. Construct layer

After the initial conditions are provided, pristine single layer graphene sheet of sizes of 125 Å by 100 Å, 250 Å by 100 Å and 500 Å by 100 Å were constructed in the *xy*-plane. First a hexagonal lattice was created, next graphene atoms were added to the lattice. Different selections of atoms are defined, which are the different boundaries needed in the next parts of the simulation.

E.1.3. Relaxation

To make sure that the system has no potential problems during computation the potential energy has to be minimised, in other words, the system must be relaxed. This step is equivalent to the relaxation step of appendix B.

E.1.4. Thermalization

The minimised system can be seen as structure being at 0 K. To run simulations at a certain temperature, the system must be thermalized. This step is equivalent to the thermalization step of appendix B.

E.1.5. Create curvature

The curvature in the graphene layers is created by moving two boundaries towards each other using the *fix move* command. As can be seen in figure E.1a the total top and bottom boundaries are moved towards each other, this done at a rate of 0.1 Å ps^{-1}. Different rates of curvature could be induced by running this step for a longer period of time. Next, the system is relaxed for 0.5 ns with the left and right boundaries fixed in all directions (figure E.1b), as if it was gripped to horizontal rollers. This relaxation is performed in the NVT ensemble. It can be seen in figure E.1c that the wrinkled configurations remain in the areas next to the

boundaries. The last step is to release the right boundary to create a cantilever structure, as can be seen in figure E.1c. The system is relaxed for 5 ns in the NVE ensemble.

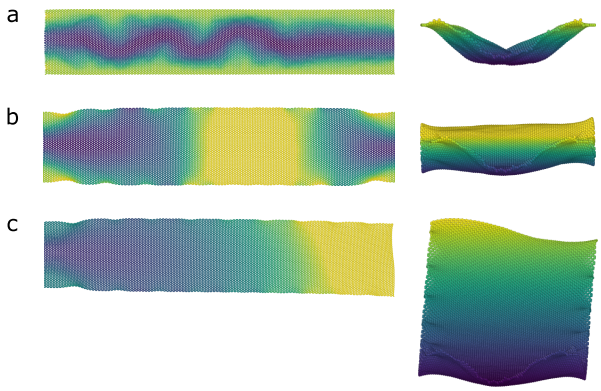

Figure E.1: The different steps in the MD model to create a curved surface: a) Moving the top and bottom boundary towards each other. b) Relax the ribbon with the right and left boundaries fixed in all directions. c) Release the right boundary to create a cantilever structure.

E.1.6. Vibration

To investigate the free vibration of the cantilever, the simulation is executed for another 5 ns in the NVT ensemble. The left boundary is still fixed in all directions and the rest of the layer is free to move.

E.2. Results of preliminary analyses

A small preliminary analysis was performed to check if, besides implying a curvature, stretching the boundary or so called 'sticking' wrinkles could also result in a stable cantilever. From the preliminary analysis on stretching it was concluded that stretching one boundary does not result in a stable layer. Another analysis was performed on sticking wrinkles. Sticking wrinkles are wrinkles which are created by moving parts of the layer towards each other up to the point were they stick to each other, as can be seen in figure E.2. The AIREBO potential is used, since this sticking is caused by van der Waals forces, which are not included in the Tersoff potential. Looking at figure E.2 it can be seen that only a small part of the displaced atoms is really sticking to the other atoms. Also, this small sticking part does not result in a stable layer. From this it was decided not to use 'sticking' wrinkles as well.

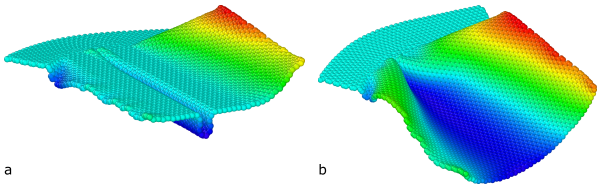

Figure E.2: Formation of sticking wrinkles. a) Snapshot just after displacement of the atoms b) Snapshot after relaxation

Bibliography

[1] The 2010 Nobel Prize in Physics - Press Release. URL https://www.nobelprize.org/nobel_prizes/physics/laureates/2010/press.html.

[2] Bekir Akgöz and Ömer Civalek. Strain gradient elasticity and modified couple stress models for buckling analysis of axially loaded micro-scaled beams. *International Journal of Engineering Science*, 49(11):1268–1280, 2011. ISSN 00207225. doi: 10.1016/j.ijengsci.2010.12.009.

[3] Deji Akinwande, Christopher J. Brennan, J. Scott Bunch, Philip Egberts, Jonathan R. Felts, Huajian Gao, Rui Huang, Joon Seok Kim, Teng Li, Yao Li, Kenneth M. Liechti, Nanshu Lu, Harold S. Park, Evan J. Reed, Peng Wang, Boris I. Yakobson, Teng Zhang, Yong Wei Zhang, Yao Zhou, and Yong Zhu. A review on mechanics and mechanical properties of 2D materials—Graphene and beyond. *Extreme Mechanics Letters*, 13:42–77, 2017. ISSN 23524316. doi: 10.1016/j.eml.2017.01.008. URL http://dx.doi.org/10.1016/j.eml.2017.01.008.

[4] R. Ansari, S. Sahmani, and B. Arash. Nonlocal plate model for free vibrations of single-layered graphene sheets. *Physics Letters, Section A: General, Atomic and Solid State Physics*, 375(1):53–62, 2010. ISSN 03759601. doi: 10.1016/j.physleta.2010.10.028. URL http://dx.doi.org/10.1016/j.physleta.2010.10.028.

[5] R. Ansari, S. Ajori, and B. Motevalli. Mechanical properties of defective single-layered graphene sheets via molecular dynamics simulation. *Superlattices and Microstructures*, 51(2):274–289, 2012. ISSN 07496036. doi: 10.1016/j.spmi.2011.11.019. URL http://dx.doi.org/10.1016/j.spmi.2011.11.019.

[6] Behrouz Arash and Quan Wang. Vibration of Single- and Double-Layered Graphene Sheets. *Journal of Nanotechnology in Engineering and Medicine*, 2(1):011012, 2011. ISSN 19492944. doi: 10.1115/1.4003353. URL http://nanoengineeringmedical.asmedigitalcollection.asme.org/article.aspx?articleid=1452547.

[7] Alexander A. Balandin. Thermal properties of graphene and nanostructured carbon materials. *Nature Materials*, 10(8):569–581, 2011. ISSN 14764660. doi: 10.1038/nmat3064. URL http://dx.doi.org/10.1038/nmat3064.

[8] Florian Banhart, Jani Kotakoski, and Arkady V. Krasheninnikov. Structural Defects in Graphene RID A-3473-2009. *Acs Nano*, 5(1):26–41, 2011. ISSN 1936-0851. doi: 10.1021/nn102598m. URL http://apps.webofknowledge.com/full_record.do?product=WOS&search_mode=CitedRefIndex&qid=3&SID=N24IB4eHeKk69MFmJan&page=2&doc=17.

[9] Wenzhong Bao, Feng Miao, Zhen Chen, Hang Zhang, Wanyoung Jang, Chris Dames, and Chun Ning Lau. Controlled ripple texturing of suspended graphene and ultrathin graphite membranes. *Nature Nanotechnology*, 4(9):562–566, 2009. ISSN 17483395. doi: 10.1038/nnano.2009.191. URL http://dx.doi.org/10.1038/nnano.2009.191.

[10] M. A. Bessa and S. Pellegrino. Design of ultra-thin shell structures in the stochastic post-buckling range using Bayesian machine learning and optimization. *International Journal of Solids and Structures*, 139-140:174–188, 2018. ISSN 00207683. doi: 10.1016/j.ijsolstr.2018.01.035. URL https://doi.org/10.1016/j.ijsolstr.2018.01.035.

[11] M. A. Bessa, R. Bostanabad, Z. Liu, A. Hu, Daniel W. Apley, C. Brinson, W. Chen, and Wing Kam Liu. A framework for data-driven analysis of materials under uncertainty: Countering the curse of dimensionality. *Computer Methods in Applied Mechanics and Engineering*, 320:633–667, 2017. ISSN 00457825. doi: 10.1016/j.cma.2017.03.037.

[12] Dw Brenner. Empirical potential for hydrocarbons for use in simulating the chemical vapor deposition of diamond films. *Physical Review B*, 42(15):9458–9471, 1990. ISSN 0163-1829. doi: 10.1103/PhysRevB.42.9458. URL http://prb.aps.org/abstract/PRB/v42/i15/p9458_1.

[13] Dale A. C. Brownson, Dimitrios K. Kampouris, and Craig E. Banks. *Graphene electrochemistry: fundamental concepts through to prominent applications*, volume 41. 2012. ISBN 1612471196. doi: 10.1039/c2cs35105f. URL http://xlink.rsc.org/?DOI=c2cs35105f.

[14] E. Cerda and L. Mahadevan. Geometry and Physics of Wrinkling. *Physical Review Letters*, 90(7):4, 2003. ISSN 10797114. doi: 10.1103/PhysRevLett.90.074302.

[15] S S Chen, A L Moore, W W Cai, J W Suk, J H An, C Mishra, C Amos, C W Magnuson, J Y Kang, and L Shi. Raman Measurements of Thermal Transport in Suspended Monolayer Graphene of Variable Sizes in Vacuum and Gaseous Environments. *ACS Nano*, 5(1):321, 2011.

[16] Shuo Chen and D. C. Chrzan. Monte Carlo simulation of temperature-dependent elastic properties of graphene. *Physical Review B*, 84(19):195409, 2011. ISSN 1098-0121. doi: 10.1103/PhysRevB.84.195409. URL https://link.aps.org/doi/10.1103/PhysRevB.84.195409.

[17] Wen Hui Duan, Kai Gong, and Quan Wang. Controlling the formation of wrinkles in a single layer graphene sheet subjected to in-plane shear. *Carbon*, 49(9):3107–3112, 2011. ISSN 00086223. doi: 10.1016/j.carbon.2011.03.033. URL http://dx.doi.org/10.1016/j.carbon.2011.03.033.

[18] A. Cemal Eringen. On differential equations of nonlocal elasticity and solutions of screw dislocation and surface waves. *Journal of Applied Physics*, 54(9):4703–4710, 1983. ISSN 00218979. doi: 10.1063/1.332803.

[19] A. S. Fedorov, D. A. Fedorov, Z. I. Popov, Yu. E. Anan'eva, N. S. Eliseeva, and A. A. Kuzubov. Mobility of vacancies under deformation and their effect on the elastic properties of graphene. *Journal of Experimental and Theoretical Physics*, 112(5):820–824, 2011. ISSN 1063-7761. doi: 10.1134/S1063776111040042. URL http://link.springer.com/10.1134/S1063776111040042.

[20] Yin Fu, Tarek Ragab, and Cemal Basaran. The effect of Stone-Wales defects on the mechanical behavior of graphene nano-ribbons. *Computational Materials Science*, 124:142–150, 2016. ISSN 09270256. doi: 10.1016/j.commatsci.2016.07.022. URL http://dx.doi.org/10.1016/j.commatsci.2016.07.022.

[21] Wei Gao and Rui Huang. Thermomechanics of monolayer graphene: Rippling, thermal expansion and elasticity. *Journal of the Mechanics and Physics of Solids*, 66(1):42–58, 2014. ISSN 00225096. doi: 10.1016/j.jmps.2014.01.011. URL http://dx.doi.org/10.1016/j.jmps.2014.01.011.

[22] I. V. Gornyi, V. Yu Kachorovskii, and A. D. Mirlin. Anomalous Hooke's law in disordered graphene. *2D Materials*, 4(1), 2017. ISSN 20531583. doi: 10.1088/2053-1583/4/1/011003.

[23] Single-layer Graphene, Alexander A Balandin, Suchismita Ghosh, Wenzhong Bao, and Irene Calizo. Superior Thermal Conductivity of. *Nano*, 2008.

[24] Joseph N. Grima, Szymon Winczewski, Luke Mizzi, Michael C. Grech, Reuben Cauchi, Ruben Gatt, Daphne Attard, Krzysztof W. Wojciechowski, and Jarosław Rybicki. Tailoring graphene to achieve negative poisson's ratio properties. *Advanced Materials*, 27(8):1455–1459, 2015. ISSN 15214095. doi: 10.1002/adma.201404106.

[25] F. Guinea, Baruch Horovitz, and P. Le Doussal. Gauge fields, ripples and wrinkles in graphene layers. *Solid State Communications*, 149(27-28):1140–1143, 2009. ISSN 00381098. doi: 10.1016/j.ssc.2009.02.044. URL http://dx.doi.org/10.1016/j.ssc.2009.02.044.

[26] Simon Van Hemert. Extracting elastic properties of graphene nanodrums using a multi-modal approach in Molecular Dynamics. 2017.

[27] M Z Hossain, T Hao, and B Silverman. Stillinger – Weber potential for elastic and fracture properties in graphene and carbon nanotubes. 2018.

[28] Jin-Wu Jiang, Tienchong Chang, Xingming Guo, and Harold S. Park. Intrinsic Negative Poisson's Ratio for Single-Layer Graphene. 2016. ISSN 1530-6984. doi: 10.1021/acs.nanolett.6b02538. URL http://arxiv.org/abs/1605.01827%0Ahttp://dx.doi.org/10.1021/acs.nanolett.6b02538.

[29] W.T. Koiter. Couple-stresses in the theory of elasticity: I and II. *Proceedings of the Koninklijke Nederlandse Akademie van Wetenschappen, Series B*, 16(I):17–44, 1964.

[30] Konstantin N. Kudin, Gustavo E. Scuseria, and Boris I. Yakobson. C2F, BN, and C nanoshell elasticity from ab initio computations. *Physical Review B*, 64(23):235406, 2001. ISSN 0163-1829. doi: 10.1103/PhysRevB.64.235406. URL https://link.aps.org/doi/10.1103/PhysRevB.64.235406.

[31] D. C.C. Lam, F. Yang, A. C.M. Chong, J. Wang, and P. Tong. Experiments and theory in strain gradient elasticity. *Journal of the Mechanics and Physics of Solids*, 51(8):1477–1508, 2003. ISSN 00225096. doi: 10.1016/S0022-5096(03)00053-X.

[32] Changgu Lee, Xiaoding Wei, Jeffrey W. Kysar, and James Hone. Measurement of the elastic properties and intrinsic strength of monolayer graphene. *Science*, 321(5887):385–388, 2008. ISSN 00368075. doi: 10.1126/science.1157996.

[33] Gun Do Lee, C. Z. Wang, Euijoon Yoon, Nong Moon Hwang, Doh Yeon Kim, and K. M. Ho. Diffusion, coalescence, and reconstruction of vacancy defects in graphene layers. *Physical Review Letters*, 95(20):1–4, 2005. ISSN 00319007. doi: 10.1103/PhysRevLett.95.205501.

[34] Seungjun Lee. Effect of Intrinsic Ripples on Elasticity of the Graphene Monolayer. *Nanoscale Research Letters*, 10(1), 2015. ISSN 1556276X. doi: 10.1186/s11671-015-1135-5. URL http://dx.doi.org/10.1186/s11671-015-1135-5.

[35] Niklas Lindahl, Daniel Midtvedt, Johannes Svensson, Oleg A. Nerushev, Niclas Lindvall, Andreas Isacsson, and Eleanor E.B. Campbell. Determination of the bending rigidity of graphene via electrostatic actuation of buckled membranes. *Nano Letters*, 12(7):3526–3531, 2012. ISSN 15306984. doi: 10.1021/nl301080v.

[36] B. Liu, Y. Huang, H. Jiang, S. Qu, and K. C. Hwang. The atomic-scale finite element method. *Computer Methods in Applied Mechanics and Engineering*, 193(17-20):1849–1864, 2004. ISSN 00457825. doi: 10.1016/j.cma.2003.12.037.

[37] Fang Liu, Pingbing Ming, and Ju Li. Ab initio calculation of ideal strength and phonon instability of graphene under tension. *Physical Review B - Condensed Matter and Materials Physics*, 76(6):1–7, 2007. ISSN 10980121. doi: 10.1103/PhysRevB.76.064120.

[38] Nan Liu, Zhonghuai Pan, Lei Fu, Chaohua Zhang, Boya Dai, and Zhongfan Liu. The origin of wrinkles on transferred graphene. *Nano Research*, 4(10):996–1004, 2011. ISSN 19980124. doi: 10.1007/s12274-011-0156-3.

[39] Qiang Lu, Marino Arroyo, and Rui Huang. Elastic bending modulus of monolayer graphene. *Journal of Physics D: Applied Physics*, 42(10), 2009. ISSN 00223727. doi: 10.1088/0022-3727/42/10/102002.

[40] Jiayan Luo, Hee Dong Jang, Tao Sun, Li Xiao, Zhen He, Alexandros P. Katsoulidis, Mercouri G. Kanatzidis, J. Murray Gibson, and Jiaxing Huang. Compression and aggregation-resistant particles of crumpled soft sheets. *ACS Nano*, 5(11):8943–8949, 2011. ISSN 19360851. doi: 10.1021/nn203115u.

[41] Jie Ma, Dario Alfè, Angelos Michaelides, and Enge Wang. Stone-Wales defects in graphene and other planar s p2 -bonded materials. *Physical Review B - Condensed Matter and Materials Physics*, 80(3):1–4, 2009. ISSN 10980121. doi: 10.1103/PhysRevB.80.033407.

[42] Bruno F. Machado and Philippe Serp. Graphene-based materials for catalysis. *Catal. Sci. Technol.*, 2 (1):54–75, 2012. ISSN 2044-4753. doi: 10.1039/C1CY00361E. URL http://xlink.rsc.org/?DOI=C1CY00361E.

[43] N A Marks. Generalizing the environment-dependent interaction potential for carbon. doi: 10.1103/PhysRevB.63.035401. URL https://journals.aps.org/prb/pdf/10.1103/PhysRevB.63.035401.

[44] Alexander S. Mayorov, Roman V. Gorbachev, Sergey V. Morozov, Liam Britnell, Rashid Jalil, Leonid A. Ponomarenko, Peter Blake, Kostya S. Novoselov, Kenji Watanabe, Takashi Taniguchi, and A. K. Geim. Micrometer-scale ballistic transport in encapsulated graphene at room temperature. *Nano Letters*, 11 (6):2396–2399, 2011. ISSN 15306984. doi: 10.1021/nl200758b.

[45] Jannik C. Meyer, A. K. Geim, M. I. Katsnelson, K. S. Novoselov, T. J. Booth, and S. Roth. The structure of suspended graphene sheets. *Nature*, 446(7131):60–63, 2007. ISSN 00280836. doi: 10.1038/nature05545.

[46] K. Min and N. R. Aluru. Mechanical properties of graphene under shear deformation. *Applied Physics Letters*, 98(1):1–4, 2011. ISSN 00036951. doi: 10.1063/1.3534787.

[47] Bohayra Mortazavi and Saïd Ahzi. Thermal conductivity and tensile response of defective graphene: A molecular dynamics study. *Carbon*, 63:460–470, 2013. ISSN 00086223. doi: 10.1016/j.carbon.2013.07.017.

[48] Nicolas Mounet and Nicola Marzari. First-principles determination of the structural, vibrational and thermodynamic properties of diamond, graphite, and derivatives. *Physical Review B - Condensed Matter and Materials Physics*, 71(20):1–14, 2005. ISSN 10980121. doi: 10.1103/PhysRevB.71.205214.

[49] M. Neek-Amal and F. M. Peeters. Graphene nanoribbons subjected to axial stress. *Physical Review B - Condensed Matter and Materials Physics*, 82(8):1–6, 2010. ISSN 10980121. doi: 10.1103/PhysRevB.82.085432.

[50] D.R. Nelson and L. Peliti. Fluctuations in membranes with crystalline and hexatic order. *Journal de Physique*, 48(7):1085–1092, 1987. ISSN 0302-0738. doi: 10.1051/jphys:019870048070108500. URL http://www.edpsciences.org/10.1051/jphys:019870048070108500.

[51] Ryan J.T. Nicholl, Hiram J. Conley, Nickolay V. Lavrik, Ivan Vlassiouk, Yevgeniy S. Puzyrev, Vijayashree Parsi Sreenivas, Sokrates T. Pantelides, and Kirill I. Bolotin. The effect of intrinsic crumpling on the mechanics of free-standing graphene. *Nature Communications*, 6:1–7, 2015. ISSN 20411723. doi: 10.1038/ncomms9789. URL http://dx.doi.org/10.1038/ncomms9789.

[52] Ryan J.T. Nicholl, Nickolay V. Lavrik, Ivan Vlassiouk, Bernadeta R. Srijanto, and Kirill I. Bolotin. Hidden Area and Mechanical Nonlinearities in Freestanding Graphene. *Physical Review Letters*, 118(26), 2017. ISSN 10797114. doi: 10.1103/PhysRevLett.118.266101.

[53] R. Nicklow, N. Wakabayashi, and H. G. Smith. Lattice Dynamics of Pyrolytic Graphite. *Phys. Rev. B*, 5(12):4951, 1972. ISSN 0556-2805. doi: 10.1103/PhysRevB.5.4951.

[54] K. S. Novoselov, A. K. Geim, S. V. Morozov, D. Jiang, M. I. Katsnelson, I. V. Grigorieva, S. V. Dubonos, and A. A. Firsov. Two-dimensional gas of massless Dirac fermions in graphene. *Nature*, 438(7065):197–200, 2005. ISSN 00280836. doi: 10.1038/nature04233.

[55] A. N. Obraztsov, E. A. Obraztsova, A. V. Tyurnina, and A. A. Zolotukhin. Chemical vapor deposition of thin graphite films of nanometer thickness. *Carbon*, 45(10):2017–2021, 2007. ISSN 00086223. doi: 10.1016/j.carbon.2007.05.028.

[56] Steve Plimpton. Fast parallel algorithms for short-range molecular dynamics, 1995. ISSN 00219991.

[57] Luka Pocivavsek, Robert Dellsy, Andrew Kern, Sebastián Johnson, Binhua Lin, Ka C Yee Lee, and Enrique Cerda. Stress and Fold Localization in Thin Elastic Membranes. *Mon. Not. R. Astron. Soc*, 40(11):1003, 2002. doi: 10.1126/science.1154923. URL www.sciencemag.org/cgi/content/full/320/5878/909/DC1.

[58] Nikolai A. Poklonski, Eugene F. Kislyakov, Sergey A. Vyrko, Oleg N. Bubel', and Sergey V. Ratkevich. Electronic band structure and magnetic states of zigzag graphene nanoribbons: quantum chemical calculations. *Journal of Nanophotonics*, 6(1):061712, 2012. ISSN 1934-2608. doi: 10.1117/1.JNP.6.061712. URL http://nanophotonics.spiedigitallibrary.org/article.aspx?doi=10.1117/1.JNP.6.061712.

[59] Huasong Qin, Yu Sun, Jefferson Zhe Liu, Mengjie Li, and Yilun Liu. Negative Poisson's ratio in rippled graphene. *Nanoscale*, 9(12):4135–4142, 2017. ISSN 2040-3364. doi: 10.1039/C6NR07911C. URL http://xlink.rsc.org/?DOI=C6NR07911C.

[60] Rinaldo Raccichini, Alberto Varzi, Stefano Passerini, and Bruno Scrosati. The role of graphene for electrochemical energy storage. *Nature Materials*, 14(3):271–279, 2015. ISSN 14764660. doi: 10.1038/nmat4170.

[61] Bipul Rakshit and Priya Mahadevan. Absence of rippling in graphene under biaxial tensile strain. *Physical Review B - Condensed Matter and Materials Physics*, 82(15):1–4, 2010. ISSN 10980121. doi: 10.1103/PhysRevB.82.153407.

[62] R. Ramírez, E. Chacón, and C. P. Herrero. Anharmonic effects in the optical and acoustic bending modes of graphene. *Physical Review B*, 93(23):1–10, 2016. ISSN 24699969. doi: 10.1103/PhysRevB.93.235419.

[63] Carlos S. Ruiz-Vargas, Houlong L. Zhuang, Pinshane Y. Huang, Arend M. Van Der Zande, Shivank Garg, Paul L. McEuen, David A. Muller, Richard G. Hennig, and Jiwoong Park. Softened elastic response and unzipping in chemical vapor deposition graphene membranes. *Nano Letters*, 11(6):2259–2263, 2011. ISSN 15306984. doi: 10.1021/nl200429f.

[64] A. Sakhaee-Pour, M. T. Ahmadian, and R. Naghdabadi. Vibrational analysis of single-layered graphene sheets. *Nanotechnology*, 19(8), 2008. ISSN 09574484. doi: 10.1088/0957-4484/19/8/085702.

[65] Virendra Singh, Daeha Joung, Lei Zhai, Soumen Das, Saiful I. Khondaker, and Sudipta Seal. Graphene based materials: Past, present and future. *Progress in Materials Science*, 56(8):1178–1271, 2011. ISSN 00796425. doi: 10.1016/j.pmatsci.2011.03.003. URL http://dx.doi.org/10.1016/j.pmatsci.2011.03.003.

[66] Wales D.J. Stone, A.J. Theoretical studies of icosahedral C60, and some related species. 128(5):501–503, 1986.

[67] Steven J Stuart, Alan B Tutein, and Judith A Harrison. A reactive potential for hydrocarbons with intermolecular interactions. *Citation: J. Chem. Phys*, 112:6472, 2000. doi: 10.1063/1.481208. URL http://aip.scitation.org/toc/jcp/112/14.

[68] A. Tapia, R. Peón-Escalante, C. Villanueva, and F. Avilés. Influence of vacancies on the elastic properties of a graphene sheet. *Computational Materials Science*, 55:255–262, 2012. ISSN 09270256. doi: 10.1016/j.commatsci.2011.12.013. URL http://dx.doi.org/10.1016/j.commatsci.2011.12.013.

[69] H. TERRONES and A.L. MACKAY. the Geometry of Hypothetical Curved Graphite Structures. *The Fullerenes*, 30(8):113–122, 1993. ISSN 00086223. doi: 10.1016/B978-0-08-042152-0.50014-4. URL http://linkinghub.elsevier.com/retrieve/pii/B9780080421520500144.

[70] Gregory Van Lier, Christian Van Alsenoy, Vic Van Doren, and Paul Geerlings. Ab initio study of the elastic properties of single-walled carbon nanotubes and graphene. *Chemical Physics Letters*, 326(1-2):181–185, 2000. ISSN 00092614. doi: 10.1016/S0009-2614(00)00764-8. URL http://linkinghub.elsevier.com/retrieve/pii/S0009261400007648.

[71] Hugues Vandeparre, Miguel Piñeirua, Fabian Brau, Benoit Roman, José Bico, Cyprien Gay, Wenzhong Bao, Chun Ning Lau, Pedro M. Reis, and Pascal Damman. Wrinkling hierarchy in constrained thin sheets from suspended graphene to curtains. *Physical Review Letters*, 106(22):3–6, 2011. ISSN 00319007. doi: 10.1103/PhysRevLett.106.224301.

[72] J. Wan, J.-W. Jiang, and H.S. Park. Irreversible crumpling of graphene from hydrostatic and biaxial compression. *Journal of Physics D: Applied Physics*, 51(1), 2018. ISSN 13616463. doi: 10.1088/1361-6463/aa99af.

[73] C. Y. Wang, K. Mylvaganam, and L. C. Zhang. Wrinkling of monolayer graphene: A study by molecular dynamics and continuum plate theory. *Physical Review B - Condensed Matter and Materials Physics*, 80(15):1–5, 2009. ISSN 10980121. doi: 10.1103/PhysRevB.80.155445.

[74] M. C. Wang, C. Yan, L. Ma, N. Hu, and M. W. Chen. Effect of defects on fracture strength of graphene sheets. *Computational Materials Science*, 54(1):236–239, 2012. ISSN 09270256. doi: 10.1016/j.commatsci.2011.10.032.

[75] Xiangyang Wang and Xu Guo. Quasi-continuum model for the finite deformation of single-layer graphene sheets based on the temperature-related higher order cauchy-born rule. *Journal of Computational and Theoretical Nanoscience*, 10(1):154–164, 2013. ISSN 15461955. doi: 10.1166/jctn.2013.2672.

[76] Yujie Wei, Baoling Wang, Jiangtao Wu, Ronggui Yang, and Martin L. Dunn. Bending rigidity and Gaussian bending stiffness of single-layered graphene. *Nano Letters*, 13(1):26–30, 2013. ISSN 15306984. doi: 10.1021/nl303168w.

[77] Wei Han and Klaus Schulten. Models.jpg (2880×1144). URL `http://www.ks.uiuc.edu/Research/cgfolding/Models.jpg`.

[78] Hongyi Xu, Yang Li, Catherine Brinson, and Wei Chen. Descriptor-Based Methodology for Designing Heterogeneous Microstructural Materials System. In *Volume 3A: 39th Design Automation Conference*, 2013. ISBN 978-0-7918-5588-1. doi: 10.1115/DETC2013-12232.

[79] P. Xu, M. Neek-Amal, S. D. Barber, J. K. Schoelz, M. L. Ackerman, P. M. Thibado, A. Sadeghi, and F. M. Peeters. Unusual ultra-low-frequency fluctuations in freestanding graphene. *Nature Communications*, 5:1–7, 2014. ISSN 20411723. doi: 10.1038/ncomms4720.

[80] Oleg V. Yazyev and Steven G. Louie. Topological defects in graphene: Dislocations and grain boundaries. *Physical Review B - Condensed Matter and Materials Physics*, 81(19):1–7, 2010. ISSN 10980121. doi: 10.1103/PhysRevB.81.195420.

[81] K. V. Zakharchenko, M. I. Katsnelson, and A. Fasolino. Finite temperature lattice properties of graphene beyond the quasiharmonic approximation. *Physical Review Letters*, 102(4):2–5, 2009. ISSN 00319007. doi: 10.1103/PhysRevLett.102.046808.

[82] Jianfeng Zang, Changyong Cao, Yaying Feng, Jie Liu, and Xuanhe Zhao. Stretchable and High-Performance Supercapacitors with Crumpled Graphene Papers. *Scientific Reports*, 4:1–7, 2014. ISSN 20452322. doi: 10.1038/srep06492.

[83] Junfeng Zhang, Jijun Zhao, and Jianping Lu. Intrinsic strength and failure behaviors of graphene grain boundaries. *ACS Nano*, 6(3):2704–2711, 2012. ISSN 19360851. doi: 10.1021/nn3001356.

[84] Y. Y. Zhang and Y. T. Gu. Mechanical properties of graphene: Effects of layer number, temperature and isotope. *Computational Materials Science*, 71:197–200, 2013. ISSN 09270256. doi: 10.1016/j.commatsci.2013.01.032.

[85] H Zhao and N.R. Aluru. Temperature and strain-rate dependent fracture strength of graphynes. *Journal of Physics D: Applied Physics*, 47(42), 2014. ISSN 13616463. doi: 10.1088/0022-3727/47/42/425301.

[86] K Zhao, K Min, and N.R. Aluru. Chirality and Size Dependent Elastic Properties of Silicene Nanoribbons under Uniaxial Tension. *Nano Letters*, (Md):1–6, 2009. doi: 10.1021/nl901448z. URL `http://www.gruppofrattura.it/ocs/index.php/ICF/icf13/paper/download/11017/10396`.